Neurobiology of Disease 127 (2019) 114–130

Contents lists available at ScienceDirect

Neurobiology of Disease

journal homepage: www.elsevier.com/locate/ynbdi

Ubiquitylome profiling of Parkin-null brain reveals dysregulation of calcium homeostasis factors ATP1A2, Hippocalcin and GNA11, reflected by altered firing of noradrenergic neurons

Key J.[a,1], Mueller A.K.[b,1], Gispert S.[a], Matschke L.[b], Wittig I.[c], Corti O.[d,e,f,g], Münch C.[h], Decher N.[b,*], Auburger G.[a,*]

[a] Exp. Neurology, Goethe University Medical School, 60590 Frankfurt am Main, Germany
[b] Institute for Physiology and Pathophysiology, Vegetative Physiology and Marburg Center for Mind, Brain and Behavior - MCMBB; Clinic for Neurology, Philipps-University Marburg, 35037 Marburg, Germany
[c] Functional Proteomics, SFB 815 Core Unit, Goethe University Medical School, 60590 Frankfurt am Main, Germany
[d] Institut du Cerveau et de la Moelle épinière, ICM, Paris, F-75013, France
[e] Inserm, U1127, Paris, F-75013, France
[f] CNRS, UMR 7225, Paris, F-75013, France
[g] Sorbonne Universités, Paris, F-75013, France
[h] Institute of Biochemistry II, Goethe University Medical School, 60590 Frankfurt am Main, Germany

ARTICLE INFO

Keywords:
Parkinson's disease
Mitochondria
Parkin
Ubiquitin
Calcium
Firing frequency

ABSTRACT

Parkinson's disease (PD) is the second most frequent neurodegenerative disorder in the old population. Among its monogenic variants, a frequent cause is a mutation in the Parkin gene (*Prkn*). Deficient function of Parkin triggers ubiquitous mitochondrial dysfunction and inflammation in the brain, but it remains unclear how selective neural circuits become vulnerable and finally undergo atrophy.

We attempted to go beyond previous work, mostly done in peripheral tumor cells, which identified protein targets of Parkin activity, an ubiquitin E3 ligase. Thus, we now used aged Parkin-knockout (KO) mouse brain for a global quantification of ubiquitylated peptides by mass spectrometry (MS). This approach confirmed the most abundant substrate to be VDAC3, a mitochondrial outer membrane porin that modulates calcium flux, while uncovering also > 3-fold dysregulations for neuron-specific factors. Ubiquitylation decreases were prominent for Hippocalcin (HPCA), Calmodulin (CALM1/CALML3), Pyruvate Kinase (PKM2), sodium/potassium-transporting ATPases (ATP1A1/2/3/4), the Rab27A-GTPase activating protein alpha (TBC1D10A) and an ubiquitin ligase adapter (DDB1), while strong increases occurred for calcium transporter ATP2C1 and G-protein subunits G(i)/G(o)/G(Tr). Quantitative immunoblots validated elevated abundance for the electrogenic pump ATP1A2, for HPCA as neuron-specific calcium sensor, which stimulates guanylate cyclases and modifies axonal slow after-hyperpolarization (sAHP), and for the calcium-sensing G-protein GNA11. We assessed if compensatory molecular regulations become insufficient over time, leading to functional deficits. Patch clamp experiments in acute Parkin-KO brain slices indeed revealed alterations of the electrophysiological properties in aged noradrenergic locus coeruleus (LC) neurons. LC neurons of aged Parkin-KO brain showed an acceleration of the spontaneous pacemaker frequency, a reduction in sAHP and shortening of action potential duration, without modulation of KCNQ potassium currents.

These findings indicate altered calcium-dependent excitability in a PARK2 model of PD, mediated by diminished turnover of potential Parkin targets such as ATP1A2 and HPCA. The data also identified further novel Parkin substrate candidates like SIRT2, OTUD7B and CUL5. Our elucidation of neuron-specific mechanisms of PD pathogenesis helps to explain the known exceptional susceptibility of noradrenergic and dopaminergic projections to alterations of calcium homeostasis and its mitochondrial buffering.

* Corresponding authors.
E-mail addresses: decher@staff.uni-marburg.de (N. Decher), auburger@em.uni-frankfurt.de (G. Auburger).
[1] Joint first authorship.

https://doi.org/10.1016/j.nbd.2019.02.008
Received 15 October 2018; Received in revised form 5 December 2018; Accepted 8 February 2019
Available online 11 February 2019
0969-9961/

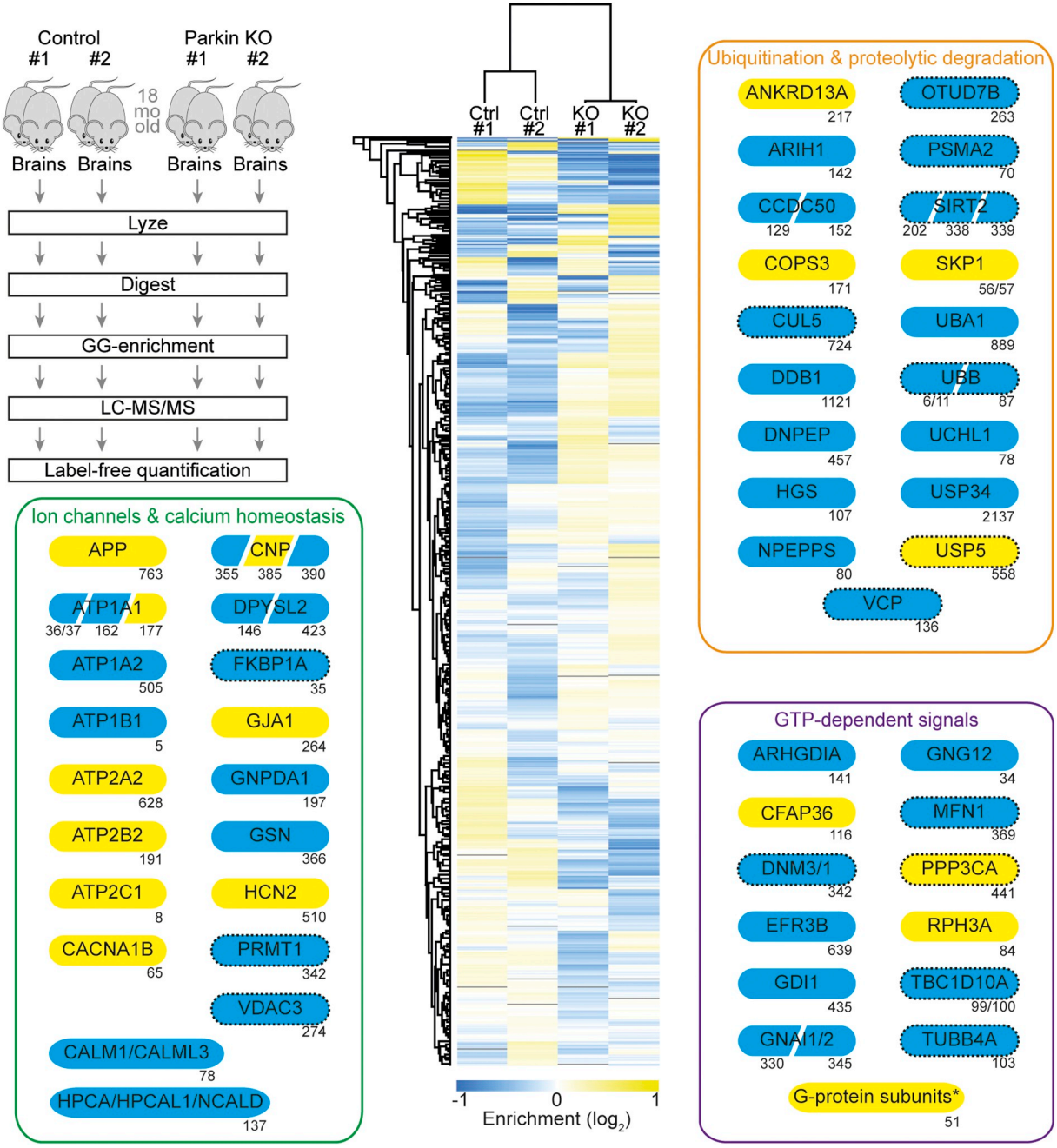

Fig. 1. Scheme of ubiquitylome profiling in old Parkin-KO brains. Study design used four male 18-month-old Parkin-KO mouse brains versus four matched controls, with pooling of brain pairs to achieve sufficient detection depth in mass spectrometry. The heat map of ubiquitin-remnant K-GG motifs for each factor with > 2-fold dysregulation illustrates sample variability and enrichment. For three significantly enriched pathways, individual factors with downregulation (blue colored symbols) or upregulation (yellow) are shown with the dysregulated ubiquitylation site (residue number). A dotted frame around the protein symbol indicates previously identified Parkin substrate candidates. Oblique white lines within the protein symbol separate ubiquitylated peptides with differential regulation. The asterisk refers to Table 1 for the identity of various G-protein subunits. (For interpretation of the references to colour in this figure legend, the reader is referred to the web version of this article.)

1. Introduction

Parkinson's disease (PD) is being intensely investigated as the second most frequent neurodegenerative disease associated with old age. Particularly a monogenic juvenile variant, PARK2, is prominent since it accounts for up to 50% of autosomal recessive familial PD cases with early onset (< 40–50 years, often before 20 years). It is characterized by relatively slow progression and a good long-term response to levodopa therapy, but frequently leads to levodopa-induced dyskinesias (Corti et al., 2011). PARK2 is caused by mutations in an E3 ubiquitin protein ligase enzyme, named Parkin, which relocalizes from the cytosol to the surface of mitochondria during cellular stress periods, thus controlling their repair, fusion-fission balance and mitophagy (Gehrke et al., 2015; Vives-Bauza et al., 2010; Ziviani et al., 2010). In view of the importance of mitochondrial dysfunction for PD pathogenesis (Lin and Beal, 2006), it is crucial to identify the ubiquitylation substrates of Parkin. Assays in vitro and co-immunoprecipitation usually in peripheral cells identified about 40 Parkin target candidates (Imai and Takahashi, 2004; Savitt et al., 2006; Seirafi et al., 2015), but in Parkin-deletion mouse brain and PARK2 patient brain the expected

accumulation of most factors could not be confirmed (Periquet et al., 2005).

The recent advent of high-throughput sequencing proteome profiling made further advances possible. In a pioneering 2D-electrophoresis and mass-spectrometry study, the ventral midbrain tissue of Parkin-deficient mice was documented to display multiple dysregulations of mitochondrial proteins and respiratory complex functions (Palacino et al., 2004). The administration of mitochondrial uncoupling agents such as CCCP or FCCP was shown to synchronize Parkin relocalization to mitochondria, permitting the identification of direct Parkin substrates among mitochondrial outer membrane proteins, such as Porin (VDAC1-3), Mitochondrial Precursor Protein Import Receptor (TOMM70A), the GTPases Mitofusin (MFN1-2), Mitochondrial Fission 1 Protein (FIS1), Dynamin-related Protein 1 (DRP1 or DNM1L), Mito-NEET (CISD1-2), Hexokinase (HK1-2), mitochondrial Rho GTPase (MIRO) and Bcl2-Associated X Protein (BAX) (Bertolin et al., 2013; Birsa et al., 2014; Gegg et al., 2010; Geisler et al., 2010; Johnson et al., 2012; Okatsu et al., 2012; Rojansky et al., 2016; Wang et al., 2011).

These substrates were later confirmed when modern approaches of quantifying ubiquitylated peptides in MS were applied to peripheral tumor cells such as HCT116 or HeLa with overexpression of Parkin (Ordureau et al., 2015a,b; Sarraf et al., 2013). Further analyses of the ubiquitylome in Parkin-mutant HeLa cells and embryonic stem-cell derived neurons have now defined the sequential steps involved in ubiquitylation dynamics at the mitochondrial outer membrane during stress periods, at least for abundant and ubiquitous Parkin substrates like VDAC1-3, CISD1-2, HK1 and MFN2 (Ordureau et al., 2018).

However, analyses of aged brain tissue by hypothesis-free global ubiquitylomics are only starting, with a pioneer project in *Drosophila melanogaster* recently confirming VDACs, CISD2, TOMM70, while identifying two dozen putative Parkin substrates that are novel and involved in vesicle dynamics rather than mitochondria (Martinez et al., 2017, 2018). A role of Parkin and its activator PINK1 for the Rab cycle of cytosolic vesicle was also substantiated by independent studies (Hammerling et al., 2017a,b; Lai et al., 2015; Song et al., 2016; Yamano et al., 2018).

Beyond these molecular details, the overall functional consequences of Parkin/PINK1 loss-of-function for the brain and motor behavior are well studied. The relevant mouse mutants show reduced spontaneous movement activity with dopaminergic deficits at advanced age (Dehorter et al., 2012; Gispert et al., 2009; Itier et al., 2003), weaker synaptic strength, paired-pulse alterations and altered long-term potentiation (Hanson et al., 2010; Kitada et al., 2007), enhanced sensitivity to group II mGlu receptor activation at corticostriatal synapses (Martella et al., 2009), altered Ca^{2+} homeostasis dependent excitability (Bishop et al., 2010; Carron et al., 2014; Gautier et al., 2016) and neuroinflammation (Mouton-Liger et al., 2018; Sliter et al., 2018; Torres-Odio et al., 2017), all of which have been explained by the mitochondrial dysfunction.

We have now undertaken a pioneer ubiquitylome survey in brain from aged Parkin-knockout (KO) and appropriately matched wildtype (WT) mice, employing an antibody against the di-glycine (K-ε-GG) remnant, which is left on ubiquitylated lysine residues after trypsin digestion, and then immuno-precipitating such peptides from the global brain proteome, in order to identify them with tandem mass spectrometry (IP-MS/MS) in a label-free quantitative manner (Fig. 1). Prominent findings were assessed in independent tissues by additional molecular techniques at the protein and mRNA level, employing the acronym of each factor in uppercase to represent the protein level in the text, while lowercase was used to represent the nucleotide level, according to NIH guidelines. Importantly, the characteristic functional consequences of such dysregulation were demonstrated by electrophysiology in acute brain slices from adult versus aged mice. Overall, the findings concur with previous reports that VDAC3 is a main target of Parkin, but also identify novel neuron-specific changes and physiological consequences that become significant only at old age.

2. Materials and methods

2.1. Mouse breeding and brain dissection

Animals were housed in individually ventilated cages with fixed light cycle under routine health monitoring at the FELASA-certified Central Animal Facility (ZFE) of the Goethe University Medical School, Frankfurt am Main. They were fed ad libitum. For dissection, mice were sacrificed by cervical dislocation. Subsequently, whole brain hemispheres were removed and frozen immediately in liquid nitrogen. Tissue was stored at −80 °C until further use. All procedures were in accordance with the German Animal Welfare Act, the Council Directive of 24 November 1986 (86/609/EWG) with Annex II, and the ETS123 (European Convention for the Protection of Vertebrate Animals). Parkin-knockout (KO) and wildtype (WT) control mice, which were derived from common ancestors and share the strain C57BL/6 genetic background, were bred among homozygotes, with genotyping as previously reported (Fournier et al., 2009; Itier et al., 2003). In all brain tissues under analysis, the genotype was controlled again by quantitative RT-PCR of the Parkin transcript level.

2.2. Global ubiquitylome

Brain hemispheres from mice at age of 18 months (four KO versus four WT matched for male sex) were dissected in parallel and shipped on dry ice for the commercial UbiScan® procedure (Cell Signaling Technology) (Kim et al., 2011; Udeshi et al., 2013). To have sufficient brain tissue for ubiquitylome profiling, always two brains of 650 mg wet weight were pooled, resulting in 4 LC-MS/MS experiments (experimental design illustrated in Fig. 1). In short, tissue extracts were protease-digested and subjected to C18 solid-phase extraction. The lyophilized peptides were immunoprecipitated by protein-A/G-agarose-immobilized ubiquitin-remnant motif antibodies #3925. Peptides were loaded directly onto a 10 cm × 75 µm PicoFrit capillary column packed with Magic C18 AQ reversed-phase resin. The column was developed with a 90 min linear gradient of acetonitrile in 0.125% formic acid delivered at 280 nl/min. The MS parameter settings were as follows: MS Run Time 96 min, MS1 Scan Range (300.0–1500.00), and Top 20 MS/MS (Min Signal 500, Isolation Width 2.0, Normalized Coll. Energy 35.0, Activation-Q 0.250, Activation Time 20.0, Lock Mass 371.101237, Charge State Rejection Enabled, Charge State 1+ Rejected, Dynamic Exclusion Enabled, Repeat Count 1, Repeat Duration 35.0, Exclusion List Size 500, Exclusion Duration 40.0, Exclusion Mass Width Relative to Mass, Exclusion Mass Width 10 ppm). MS/MS spectra were evaluated using SEQUEST 3G and the Sorcerer 2 platform from Sage-N Research (v4.0, Milpitas, CA, USA) [36]. Searches were performed against the most recent update of the NCBI *Mus musculus* database with mass accuracy of ± 50 ppm for precursor ions and 1 Da for product ions. Results were filtered with mass accuracy of ± 5 ppm on precursor ions and presence of the intended motif (Me-R). Peptide identification with relative quantification by mass spectrometry occurred by LC-MS/MS analysis using LTQ-Orbitrap-VELOS with ESI-CID Sorcerer search.

Bioinformatic processing used the maximum % coefficient of variation (% CV) to control replicate reproducibility. Using a 5% default false positive rate to filter the Sorcerer results, this procedure yielded a total of 6746 redundant ubiquitinated peptide assignments to 3427 nonredundant ubiquitinated peptides. The quantitative data from the four KO and four WT mice were pooled to derive the respective fold change. The original data are available from the authors upon request.

2.3. Bioinformatic analyses

For protein-protein interaction (PPI) network analysis, the software tool String v.10 (https://string-db.org/) with standard settings was employed to visualize networks of relevant dysregulations as previously described (Torres-Odio et al., 2017). As recommended, gene symbols of

factors with > 2-fold dysregulation were entered into the Multiple Proteins window with the *Mus musculus* option, the matching of the input with the correct factors was accepted, and the graphic interaction diagram was generated and archived. The Analysis button generated automated network statistics; significant functional enrichments of GO (Gene Ontology) terms and KEGG pathways were exported to EXCEL files.

2.4. Quantitative immunoblotting

Total proteins from 4 WT versus 4 Parkin-KO mouse brain hemispheres were isolated as described, with modifications (Lastres-Becker et al., 2016). Frozen tissues were homogenized on ice with a Dounce grinder and homogenates were lysed in RIPA buffer with 50 mM Tris-HCl (pH 8.0), 150 mM NaCl, 1% NP-40, 0.5% Na-deoxycholate, 0.1% SDS and protease inhibitor cocktail (Roche), respectively. Total lysates were briefly sonicated on ice, and cell debris was removed by centrifugation. Samples of 20 µg were heated at 90 °C for 5 min and then separated in tris–glycine polyacrylamide gels, using Precision Plus Protein™ All Blue Standards as size marker. Transfer to nitrocellulose membranes (Protran, GE Healthcare) was done at 50 V for 90 min, with blocking in 5% BSA solution in 1 × TBS-T for 1 h at room temperature (RT). Incubation with primary antibodies against HPCA (1:1000, ab24560, Abcam), ATP1A2 (1:1000, MA3–928, Thermo Scientific), GNA11 (1:1000, GTX54123, GeneTex) and β-Actin (1:5000, A5441, Sigma-Aldrich) occurred in 1 × TBS-T solutions overnight at 4 °C. Fluorescent-labeled α-mouse (Li-Cor IRDye 800CW, 1:15.000) and α-rabbit (Li-Cor IRDye 680RD, 1:15.000) were secondary antibodies, with fluorescence detection by Li-Cor Odyssey Classic Instrument.

2.5. Quantitative reverse-transcriptase polymerase chain reaction

Total RNA of 4 WT and 4 Parkin-KO mouse brain hemispheres was extracted with TRI reagent (Sigma) and cDNA was made with the Superscript IV Kit (Invitrogen), both following the manufacturer's instructions. Quantitative reverse-transcriptase (RT) polymerase chain reaction (qPCR) was performed with TaqMan Gene Expression Assays (Applied Biosystems) in cDNA from 20 ng total RNA in 20 µl reactions with 2 × master mix from Roche in a StepOnePlus Real-Time PCR system (Applied Biosystems). All assays were normalized against *Tbp* expression levels. The analysis of the data was carried out with the $2^{-\Delta\Delta CT}$ method (Livak and Schmittgen, 2001). The following TaqMan Assays were employed: *Atp1a1*-Mm00523255_m1, *Atp1a2*- Mm00617899_m1, *Atp1a3*-Mm00523430_m1, *Atp1b1*- Mm00437612_m1, *Atp2a1*-Mm01275320_m1, *Atp2a2*- Mm01201431_m1, *Atp2b2*- Mm00437640_m1, *Atp2b3*-Mm01191090_m1, *Atp2c1*- Mm00723484_m1, *Calm1*- Mm00486655_m1, *Gdi1*- Mm00802649_m1, *Gna11*- Mm01172792_m1, *Gnai1*-Mm01165301_m1, *Gnai2*- Mm00492379_g1, *Gnai3*- Mm00802670_m1, *Gnao1*- Mm00494677_m1, *Gnaz*- Mm01150269_m1, *Gng12*- Mm011-838112_m1, *Hpca*- Mm00650703_m1, *Park2*- Mm00450186_m1 and *Tbp*-Mm00446973_m1.

2.6. Dissection of vital brainstem slices

The slice dissection, electrophysiological analyses and neurobiotin immunostaining of LC neurons were performed as previously described (Matschke et al., 2018). Briefly, mice were anesthetized with isoflurane gas/intraperitoneal ketamine. They were perfused transcardially with an ice-cold glucose/magnesium-rich preparation [in mM: 2.5 KCl, 1.25 NaH_2PO_4, 10 $MgSO_4$, 20 PIPES, 10 Glucose, 200 Saccharose, 0.5 $CaCl_2$, pH 7.35] to ensure tissue vitality and brains were removed rapidly.

Coronal sections (180–200 µm thick) were made using a Campden MA752 vibratome (Campden Instruments) within the ice-cold preparation. After sectioning, slices were maintained at 30 °C for 30 min and afterwards at RT for 30 min, submerged in artificial cerebrospinal fluid (ACSF) composed of (in mM): 125 NaCl, 2.5 KCl, 25 $NaHCO_3$, 1.25 NaH_2PO_4, 2 $CaCl_2$, 1 $MgCl_2$ and 25 glucose, equilibrated to pH 7.4 with 95% O_2/5% CO_2. Subsequently, slices were kept at RT for up to 5 h. For electrophysiological recordings slices were transferred to a recording chamber mounted on an upright microscope and continuously perfused with ACSF, unless specified otherwise. LC neurons were visualized with a Zeiss AxioCam MRm camera (Carl Zeiss Microscopy, LLC, USA) mounted on a Zeiss Examiner.D1 microscope (Carl Zeiss Microscopy, LLC, USA), equipped with a 40 × /0.75 phase contrast, water immersion objective, standard EGFP filter and Texas red filter sets. Brainstem slices containing a clearly defined LC at the edge of the fourth ventricle were used for the experiments.

2.7. Slice patch clamp recordings

Patch clamp recordings were performed at RT in LC neurons identified by their large somata and pacemaker frequencies between 1 and 5 Hz. Patch pipettes were prepared from borosilicate glass capillaries GB 150TF-8P (Science Products, Hofheim, Germany), and had tip resistances between 3 and 5 MΩ. Conventional tight seal whole-cell voltage clamp experiments were conducted with ACSF as external solution and an internal solution containing (in mM): 135 K-Glutamate, 5 KCl, 10 HEPES, 0.1 EGTA, 2 $MgCl_2$, 2 MgATP, 0.2 Li_2GTP and adjusted to pH 7.4 with KOH. All patch clamp recordings were made using a Multiclamp 700B amplifier (Molecular Devices, Sunnyvale CA, USA) and Clampex 10.0 software (Molecular Devices, Sunnyvale CA, USA). Data were digitized at 10 kHz with a Digidata 1440A digitizer (Molecular Devices, Sunnyvale CA, USA) and filtered at 1–5 kHz. Electrode capacitance was compensated and only recordings with a constant series resistant < 30 MΩ were used for analysis. All experiments were done in several mutant animals and controls (N = 3–6).

2.8. Immunostaining

For neurobiotin (NB) stainings, LC neurons were filled by adding 0.1% (*w/v*) NB to the pipette solution. After finishing patch clamp recordings, slices were subsequently fixed in a solution composed of 4% PFA in 0.1 M phosphate buffered saline (PBS), pH 7.4. After fixation for 48 h, slices were stored in 30% sucrose in 0.1 M PBS at 4 °C. For the subsequent immunohistochemical staining, sections were blocked in 10% horse serum followed by overnight incubation with primary anti-tyrosine-hydroxylase antibody (Calbiochem, #657012, working dilution 1:1000). Anti-Rabbit Alexa 568 (Invitrogen, #A11011, working dilution 1:750) served as secondary antibody and co-staining was performed with streptavidin conjugated with Alexa 488 (Invitrogen, #S11223, working dilution 1:1000).

Images were acquired with an Axio Observer.Z1 microscope (Carl Zeiss Microscopy, LLC, United States) equipped with standard EGFP filter and Texas red filter sets and an Axio Cam MRm camera (Carl Zeiss Microscopy, LLC, United States). Digital images were processed using ZEN 2.3 (Carl Zeiss Microscopy, LLC, United States).

2.9. Statistical analyses

Data are reported as means ± S.E.M. For expression studies, statistical significance was assessed using unpaired Student's *t*-test in the GraphPad Prism 7 software. For electrophysiological studies, data were analyzed using Microsoft Excel and OriginPro (OriginLab Corp., Guangzhou, China). Data sets were tested for Normality using the Shapiro Wilk test and for equal variances using the Levene's test. In normally distributed data sets, statistical significance was calculated using paired or unpaired Student's *t*-test. Otherwise non-parametric statistical tests, e.g. the Wilcoxon signed-rank test for paired data or the Mann-Whitney-*U* test for unpaired data were used. * stands for $P < .05$; ** for $P < .01$; *** for $P < .001$.

Table 1
Global ubiquitylome profile of brain from 18-month-old Parkin-KO mice. The table illustrates factors (yellow background for known Parkin substrates) and their relevant ubiquitylation sites (highlighted by asterisk) with > 2-fold dysregulation (red background for increases, blue background for decreases) and literature references. Potential novel Parkin substrates that are not neuron-specific were highlighted with light yellow background. Potential novel Parkin substrates that are neuron-specific and showed > 4-fold downregulation were highlighted with purple background. Putative compensatory upregulations of G-protein subunits were highlighted with green background.

		Normalized Fold Change	
Gene Name	**Peptide**	**KO : Control**	**Literature**
Ubiquitination and proteolytic degradation			
DDB1	MQEVVANLQYDDGSGMK*R	-3.7	Lee-J & Zhou-P 2007 Mol Cell
SIRT2	DVAWLGDCDQGCLALADLLGWKK*ELEDLVR	-3.6	Guedes-Dias-P et al 2013 BBA Outeiro-TF et al 2007 Science Tashiro-K 2006 J Biol Chem
CCDC50	HTPEFSGGSVFGDNYYHEDGGMK*PR	-3.4	Bohgaki-M et al 2008 BBA
USP34	YTFNMVTMMK*EK	-3.2	Lui-TT 2011 Mol Cell Biol
SIRT2	DVAWLGDCDQGCLALADLLGWK*KELEDLVRR	-2.7	Guedes-Dias-P et al 2013 BBA
CUL5	TQEAIIQIMK*MR	-2.7	Okumura-F 2016 Cell Div
OTUD7B	ESGLVYTEDEWQKEWNELIK*LASSEPR	-2.7	Wang-B et al 2017 Nature
UCHL1	QIEELKGQEVSPK*VYFMK	-2.7	Ferrer-I 2009 Prog Neurobiol
VCP	IHVLPIDDTVEGITGNLFEVYLK*PYFLEAYRPIR	-2.6	Sarraf-SA et al 2013 Nature
PSMA2	SVHKVEPITK*HIGLVYSGMGPDYR	-2.5	Sarraf-SA et al 2013 Nature
DNPEP	ETACTTGVLQTLTLFK*GFFELFPSVSR	-2.5	Chen-Y 2012 J Biol Chem
HGS	K*ILYLIQAWAHAFR	-2.3	Katz-M et al 2002 Traffic
UBA1	LIAGK*IIPAIATTTAAVVGLVCLELYK	-2.1	Wang-YC 2013 Zhongguo Zhen Jiu
NPEPPS	LPAEVSPINYSLCLKPDLLDFTFEGK*LEAAAQVR	-2.2	Karsten-SL 2006 Neuron Tashiro-K 2006 J Biol Chem
CCDC50	K*HTPEFSGGSVFGDNYYHEDGGMKPR	-2.0	Bohgaki-M et al 2008 BBA
SIRT2	K*EYTMGWMK	-2.0	Guedes-Dias-P et al 2013 BBA
UBB;UBC;RPS27A;UBA52	MQIFVK*TLTGK*TITLEVEPSDTIENVK	-2.0	Lim-KL 2006 Neurobiol Aging
UBB;UBC	GGMQIFVKTLTGK*TITLEVEPSDTIENVK	-2.0	Lim-KL 2006 Neurobiol Aging
ARIH1	ILLSHFNWDKEK*LMER	-2.0	Aguilera-M et al 2000 Genetics
ANKRD13A	LTLDLM#K*PK	3.2	Tanno-H et al 2012 Mol Biol Cell
COPS3	CFKPALPYLDVDM#M#DICK*ENGAYDAK	2.6	Yoneda-Kato-N 2005 EMBO J
SKP1	TM#LEDLGM#DDEGDDDPVPLPNVNAAILK*K*	2.3	Halbach-MV 2015 PLOS ONE
USP5	SVAVK*TTR	2.0	Sarraf-SA et al 2013 Nature
Ion channels & calcium homeostasis			
VDAC3	NFNAGGHK*VGLGFELEA	-8.8	Sarraf-SA et al 2013 Nature
HPCA;HPCAL1;NCALD	MVSSVMK*MPEDESTPEKR	-4.7	
CALM1;CALML3	KMK*DTDSEEEIREAFR	-4.2	
ATP1A1;ATP1A3;ATP1A4	IMESFK*NMVPQQALVIR	-3.8	
DPYSL2	TISAK*THNSALEYNIFEGMECR	-3.5	
DPYSL2	SCCDYSLHVDITEWHK*GIQEEMEALVK	-2.5	
FKBP1A	RGQTCVVHYTGMLEDGK*K	-2.4	Sarraf-SA et al 2013 Nature
ATP1A2	EDSPQSHVLVMK*GAPER	-2.3	
PRMT1	TGEEIFGTIGMRPNAK*NNR	-2.3	Kim-HJ et al 2016 Elife
GSN	TASDFISK*MQYPR	-2.1	
CNP	KMEVK*AIFTGYYGK	-2.1	
CNP	AHVTLGCAADVQPVQTGLDLLDILQQVK*GGSQGEAVGELPR	-2.0	
ATP1B1	GK*AKEEGSWKK	-2.0	
ATP1A1	DMDELK*K*EVSMDDHK	-2.0	
GNPDA1	VPTMALTVGVGTVM#DAK*EVM#ILITGAHK	-2.0	
ATP2C1	FQK*IPNVENETM#IPVLTSK	7.2	
APP	M#QQNGYENPTYK*FFEQM#QN	4.7	
CNP	WM#LSLTK*K	2.6	
GJA1	DCGSPK*YAYFNGCSSPTAPLSPM#SPPGYK	2.3	
ATP1A1	NGEK*M#SINAEDVVVGDLVEVK	2.2	
ATP2B2	IEQEQK*FTVVR	2.2	
CACNA1B	TM#ALYNPIPVK*QNCFTVNR	2.1	
ATP2A2	VIM#ITGDNK*GTAVAICR	2.1	
HCN2	K*LVASM#PLFANADPNFVTAM#LTK	2.0	
GTP-dependent signals			
TBC1D10A	WLDMLNNWDKWMAK*K*	-3.7	Yamano-K et al 2014 Elife
MFN1	NQMNLLTLDVKK*	-2.8	Sarraf-SA et al 2013 Nature
GDI1	MAGSAFDFENMK*R	-2.3	
GNAI1;GNAI2	NVQFVFDAVTDVIIK*NNLKDCGLF	-2.2	
GNAI1;GNAI2	EIYTHFTCATDTK*NVQFVFDAVTDVIIKNNLK	-2.2	
EFR3B	KKEAPYMLPEDVFVEK*PR	-2.2	
TUBB4A	SGPFGQIFRPDNFVFGQSGAGNNWAK*GHYTEGAELVDAVLDVVR	-2.2	Sarraf-SA et al 2013 Nature
DNM3;DNM1	ALLQMVQQFAVDFEK*R	-2.1	Sarraf-SA et al 2013 Nature
GNG12	IKVSK*ASADLMSYCEEHAR	-2.0	
ARHGDIA	IDK*TDYMVGSYGPR	-2.0	
G-alpha1(i);G-alpha2(i);G-alpha3(i); GNAO1;GNAT2;GNAT1;GNAT3; G-alpha(z)	STIVK*QM#K	5.4	Ghahremani-MH 2000 Mol Cell Biol Gazi-L et al 2003 Br J Pharmacol Laliberté-B et al 2010 J Cell Physiol
CFAP36	AM#M#VQK*NIEM#QLQAIR	2.8	
PPP3CA	GLTPTGM#LPSGVLSGGK*QTLQSAIK	2.2	Martinez-A 2017 Mol Neurodegener

(*continued on next page*)

Table 1 (*continued*)

RPH3A	K*NVAGDGVNR	2.2	
Vesicle dynamics			
ATP6V1A	EHMGEILYK*LSSMK	-2.8	Martinez-A 2017 Mol Neurodegener
HSPA8	DKVSSK*NSLESYAFNMK	-2.5	Sarraf-SA et al 2013 Nature
TOM1L2	NNPPTIVQDK*VLALIQAWADAFR	-2.4	
SNAP25	IEEGMDQINKDMK*EAEK*	-2.2	
SV2A	FFLENGK*HDEAWMVLK	-2.1	
SNX1	YLETLLHSQQQLAK*YWEAFLPEAK	-2.1	Song-P et al 2016 J Neurosci
SYT2	DMK*GGQDDDDAETGLTEGEGEGEEEKEPENLGK	-2.0	
SCFD1	K*SPFQEAIVFVVGGGNYIEYQNLVDYIK	-2.0	
ESYT1	DKYVK*GLIEGK	-2.0	
HSPA8	NQVAM#NPTNTVFDAK*R	2.7	Sarraf-SA et al 2013 Nature
SLC2A3	AFEGQAHSGK*GPAGVELNSM#QPVKETPGNA	2.7	
SLC17A7	YIEDAIGESAK*LM#NPVTK	2.4	
VAT1	ISPK*GVDIVM#DPLGGSDTAK	2.2	
TOM1	FRTGQTAK*ASSEAELATDLIDM#GPDPAATNNLSSQLAGM#NLGSF	2.1	
SCAMP1	AQQEFATGVM#SNK*TVQTAAANAASTAATSAAQNAFK	2.0	
SCAMP1	TVQTAAANAASTAATSAAQNAFK*GNQM#	2.0	
Phosphorylation signals			
PKM	PK*PHSEAGTAFIQTQQLHAAMADTFLEHMCR	-3.9	Sarraf-SA et al 2013 Nature
YWHAB	TAFDEAIAELDTLNEESYK*DSTLIM#QLLR	-2.8	
YWHAG	AYSEAHEISK*EHMQPTHPIR	-2.7	
YWHAQ	KQTIENSQGAYQEAFDISKK*EMQPTHPIR	-2.4	
PGK1;PGK2	VDFNVPM#K*NNQITNNQR	2.6	Sarraf-SA et al 2013 Nature
CKB	VISMQK*GGNM#K	2.4	Martinez-A 2017 Mol Neurodegener
YWHAE	DNLTLWTSDM#QGDGEEQNK*EALQDVEDENQ	2.3	Sarraf-SA et al 2013 Nature
CCK5	LPDYK*PYPM#YPATTSLVNVVPK	2.1	
Glycolysis versus respiration			
COX7A2	GGASDALLYRATMALTLGGTAYAIYLLAM#AAFPK*KQ	-3.0	
GPI	VWFVSNIDGTHIAK*TLASLSPETSLFIIASK	-2.6	
PGAM1	SYDVPPPPMEPDHPFYSNISK*DRR	-2.6	
ATP5B	IMNVIGEPIDERGPIK*TK*	-2.3	Sarraf-SA et al 2013 Nature
HDAC11	AHDIPILMVTSGGYQK*R	-2.2	Guedes-Dias-P et al 2013 BBA
COX7A2	GGASDALLYRATM#ALTLGGTAYAIYLLAM#AAFPKK*Q	-2.2	
TKT	NMAEQIIQEIYSQVQSKKK*	-2.1	
ENO1	KVNVVEQEKIDK*LMIEMDGTENK	-2.1	Sarraf-SA et al 2013 Nature
ALDOC	IVTPGK*GILAADESVGSM#AK	2.2	
Diverse pathways, autophagy, cytoskeleton, nucleus			
CNTRL	FRDEM#ENADLGAKGANSQLLEIEALNEAM#AK*	-3.4	
GLTP	QIETGPFLEAVAHLPPFFDCLGSPVFTPIK*ADISGNITK*	-3.2	
BCAS1	ADSVCDGHAAGQK*MSETQAK	-3.0	
CTNNA2	AHVLAASVEQATQNFLEKGEQIAK*ESQDLKEELVAAVEDVR	-2.7	
PEG10	NVK*DGLMTPTVAPNGAQVLQVK*R	-2.6	
ACTB;ACTA2;ACTC1; ACTG1;ACTG2;ACTA1	HQGVMVGMGQK*DSYVGDEAQSK*R	-2.6	
HSPA12A	IIIPQDVGLTILK*GAVLFGLDPAVIK	-2.3	
HINT3	QDSYWFVTVDYLLEK*LRK*	-2.1	
FSD1	LK*EDHPWMVVEGIR	-2.1	
ACTB;ACTA2;ACTC1; ACTG1;ACTG2;ACTA1	HQGVMVGMGQK*DSYVGDEAQSK*R	-2.0	
GLUL	GIK*QMYMSLPQGEK	-2.1	
QDPR	GAVHQLCQSLAGK*NSGM#PPGAAAIAVLPVTLDTPMNRK	-2.0	Si-Q 2017 Acta Biochim Biophys Sin
HIST2H2AA1;HIST2H2AC	HLQLAIRNDEELNKLLGKVTIAQGGVLPNIQAVLLPKK*	-2.0	
MED25;MED9	TAPCEVRVLMLLYSSKK*	-2.0	
TXNL1	LYSM#K*FQGPDNGQGPK	2.8	
EEF1A1	SGDAAIVDM#VPGK*PM#CVESFSDYPPLGR	2.7	
PSAT1	FLDK*AVELNM#ISLK	2.4	
QDPR	EGGLLTLAGAK*AALDGTPGM#IGYGM#AK	2.4	Si-Q 2017 Acta Biochim Biophys Sin
PSAT1	FLDK*AVELNM#ISLK	2.4	
SYCP3	NNDNLFTGTQSELK*KEM#AMLQK	2.2	

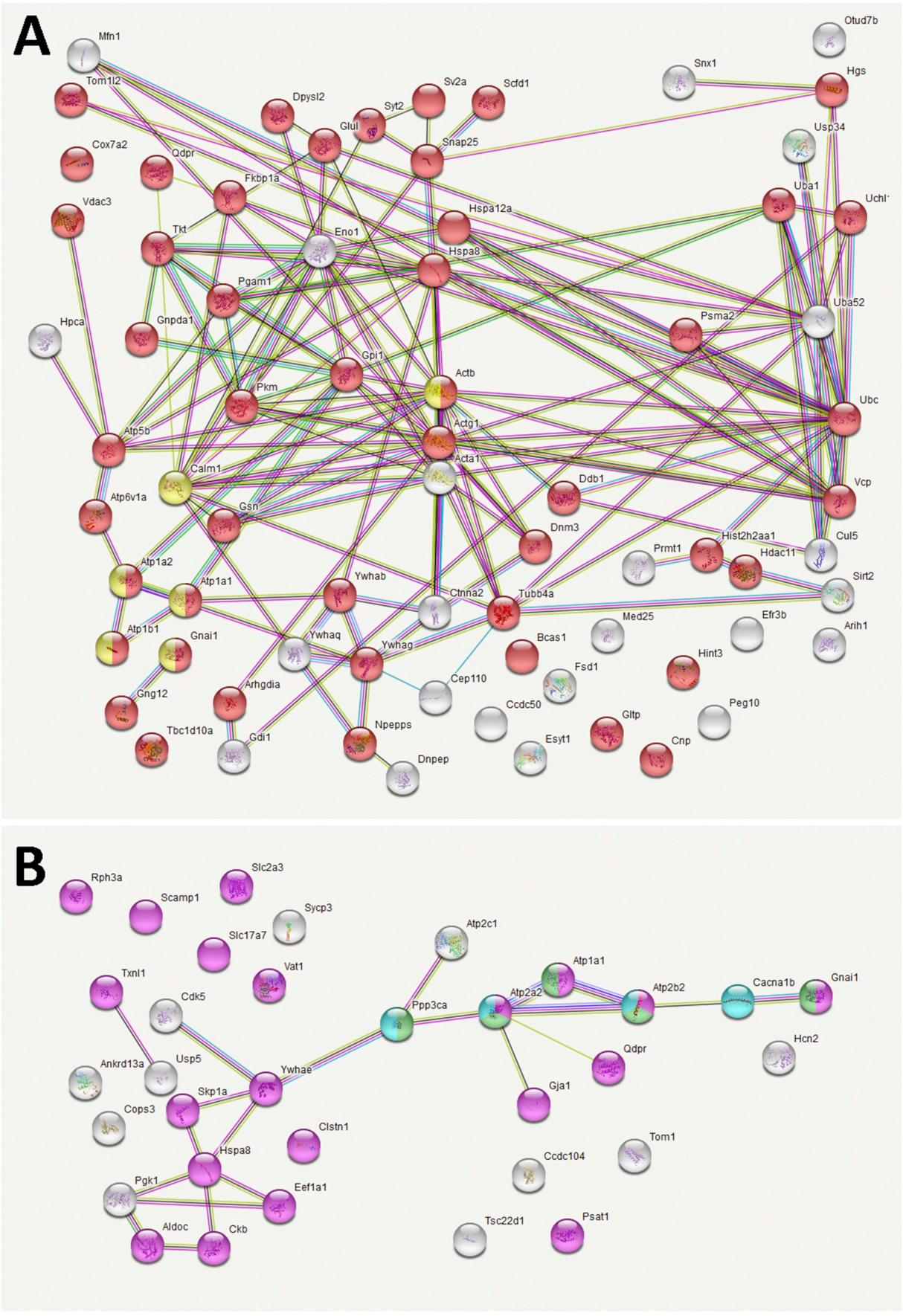

(caption on next page)

Fig. 2. Diagram of protein-protein interactions among the factors with ubiquitylation changes beyond two-fold, according to the STRING website. **(A)** All downregulations are shown, with factors involved in ubiquitin and protein turnover placed on the right upper margin, those involved in mitochondrial function placed into the left upper margin, Hippocalcin at the left middle margin. Red symbols indicate vesicle-associated factors, while yellow symbols illustrate factors that are relevant for stimulus-dependent acid secretion, with Calmodulin among them. **(B)** All upregulations are shown, with factors involved in secretory vesicles placed into the left upper corner. Purple symbols indicate proteins at membrane-bounded vesicles, e.g. the Rab3a-interactor Rph3a in the upper left corner. Light blue stands for the calcium signaling pathway, including several calcium channels. Light green illustrates the cGMP PKG signaling pathway components, e.g. Gnai1 placed at the right margin. (For interpretation of the references to colour in this figure legend, the reader is referred to the web version of this article.)

3. Results

3.1. Aged Parkin-KO brain ubiquitylome profile overview

3.1.1. Downregulations were prominent

The brain ubiquitylome of 18-month-old Parkin-KO mice showed 114 peptide dysregulations that had > 2-fold effect size (Table 1), including 21 known Parkin substrates (highlighted by yellow background in Table 1). Downregulation of 79 ubiquitylation sites was documented (highlighted by blue background in Table 1), providing a promising basis to identify novel neuron-specific direct Parkin ubiquitylation targets among additional indirect effects. Interestingly, 34 upregulations were also observed (highlighted by red background in Table 1), which may represent random consequences of the perturbed protein degradation machinery as well as compensatory efforts.

3.1.2. Some factors harbored both down- and upregulations

Downregulations and possibly homeostatic upregulations coincided in selected factors (shown as symbols with blue and yellow colour in Fig. 1), in particular a moderate ubiquitylation deficit of a peptide from GNAI1/GNAI2 (−2.2-fold at amino acid §345/346 and at §330/331) was observed together with a strongly increased ubiquitylation (+5.4-fold at §47/51) of a peptide from the G-protein subunits GNAI1/GNAI2/GNAI3/GNAO1/GNAT1/GNAT2/GNAT3/GNAZ, highlighted with green background in Table 1. Similarly, an ubiquitylation deficit in a peptide from ATP-driven Na/K-pumps ATP1A1/ATP1A3/ATP1A4 (−3.8-fold at §152/162/172) and in a peptide purely from ATP1A1 (−2.0-fold at §36/37) contrasted with an excessive ubiquitylation of ATP1A1 (+2.2-fold at §177). Furthermore, an ubiquitylation deficit in the immunity modifier (Girirajan et al., 2008) and ubiquitin/clathrin/Tollip interactor TOM1L2 (−2.4-fold at §116) occurred together with excessive ubiquitylation of its homolog TOM1 (+2.1-fold at §311). In addition, an ubiquitylation deficit in the autophagy modulator QDPR at §164 (−2.0-fold) accompanied an excessive ubiquitylation of QDPR at §135 (+2.4-fold). Finally, an ubiquitylation deficit in CNP (−2.0-fold at §335/355; −2.1-fold at §370/390) was observed in parallel with excessive ubiquitylation in CNP (+2.6-fold at §365/385) and might influence its association with Calmodulin and its mitochondrial regulation in response to calcium (Azarashvili et al., 2009; Myllykoski et al., 2012). In these proteins it may be crucial for the cell to maintain the steady-state levels normal, so that indirect compensatory efforts counterweigh the pathological ubiquitylation deficits triggered by Parkin deficiency.

3.1.3. The 3 biggest downregulations occurred in calcium regulators

Focusing primarily on the strongest downregulations (beyond −4.0-fold cutoff), an exceptional −8.8-fold ubiquitylation deficit was observed for VDAC3 as member of the Porin family and as known Parkin substrate, reproducing previous reports and confirming the validity of our approach. This protein family controls mitochondrial calcium homeostasis at the mitochondrial outer membrane, which is crucial when neuronal pacemaker activity changes due to stimulation, with subsequent increases of energy demand (Cali et al., 2014; Surmeier et al., 2012). A peptide from the neuron-specific calcium sensors Hippocalcin, Hippocalcin-Like 1 or Neurocalcin Delta (HPCA, HPCAL1 or NCALD) showed the second strongest effect (−4.7-fold), and a peptide from the calcium-buffering factors Calmodulin or Calmodulin-Like 3 (CALM1 or CALML3) showed a third substantial effect (−4.2-fold). Given that mitochondrial dysfunction in Parkin-deficient brain may alter the mitochondrial calcium storage and calcium-dependent excitability of neurons, it is possible that Hippocalcin and Calmodulin change due to indirect cellular adaptations rather than as direct Parkin substrates, but these findings had high credibility and were investigated further by quantitative RT-PCR, quantitative immunoblots and electrophysiology.

3.2. The KO brain ubiquitylome contains > 2-fold downregulation of 15 known PARKIN substrates

3.2.1. Several established Parkin ubiquitylation targets were confirmed

It was important to note that the ubiquitylation of overall cellular pools of ubiquitin (UBB/UBC) as a known Parkin substrate changed −2.0-fold, an observation with consequences for the turnover of practically all proteins. Therefore, in subsequent bioinformatics analyses only effects that surpassed this threshold were taken into account. Apart from VDAC3 (−8.8-fold) and UBB/UBC (−2.0), the downregulation of other known Parkin substrates ranged from −3 to −2 fold levels (overview in Fig. 1). This included the calcium release modulator FKBP1A (−2.4); several GTPases, such as the mitochondrial fusion factor MFN1 (−2.8), the microtubule and LRRK2 interactor TUBB4A (−2.2) and the vesicle endocytosis factors DNM1/DNM3 (−2.1); the vesicle ATPase ATP6V1A (−2.8), the Golgi vesicle ATPase VCP (−2.6) and the vesicular trafficking modulator SNX1 (−2.1); the molecular chaperone HSPA8 (−2.5 at §539, but +2.7 at §71) and the proteasome subunit PSMA2 (−2.5); the glycolytic kinase PKM (−3.9), the glycolytic enzyme ENO1 (−2.1) and the respiratory ATP synthase subunit ATP5B (−2.3) (relevant literature references in Table 1).

3.2.2. Four ubiquitylation downregulations may represent novel Parkin targets

Four factors hold immediate promise as novel potential Parkin substrates in view of their involvement in PD pathogenesis, although they are not neural-specific: First, a strongly decreased ubiquitylation (−3.6-fold at §339/302/269, −2.7 at §338/301/268 and − 2.0-fold at §202/202/165/132) was observed for SIRT2, which is a target of Cbl-dependent ubiquitylation during EGFR-endocytosis, deacetylates the p65 subunit of NF-kB and protects against Parkinsonian alpha-synuclein neurotoxicity (Outeiro et al., 2007). It also deacetylates the transcriptional factor FOXO3 to stimulate its SCF(SKP2)-mediated ubiquitination, in a pathway that modulates dopaminergic differentiation as well as nigrostriatal vulnerability to the neurotoxin MPTP (Liu et al., 2012; Pino et al., 2014; Szego et al., 2017), via AKT/GSK-3β/β-catenin. Second, the reduced ubiquitylation of a modulator of bacteria-containing endosomes and autophagy (Minowa-Nozawa et al., 2017), the RAB35-associated, GTPase activating protein TBC1D10A (−3.7 at §99 and §100) may hold particular interest, since TBC1D15 as another RabGAP was already documented to act downstream of Parkin (Yamano et al., 2018). Third, the reduced ubiquitylation of the deubiquitinase OTUD7B (−2.7-fold at §263) may deserve special attention, given that it acts as inhibitor of NF-kB via the known Parkin-substrate TRAF3 (TNF Receptor Associated Factor 3, a RING-Type E3 Ubiquitin Transferase), as modulator of mTOR-dependent growth together with TRAF2, and as modifier of EGFR turnover (Pareja et al., 2012; Wang et al., 2017; Xin et al., 2018). Fourth, the reduced ubiquitylation of the

ubiquitin ligase scaffold CUL5 (−2.7-fold at §724, also named VACM-1 for its vasopressin-dependent action on calcium mobilization and cAMP production) is meaningful in this context, given that CUL5 interacts with TRAF6 to promote lipopolysaccharide signals (Zhu et al., 2016), which are known to exacerbate Parkin-dependent pathology (Tran et al., 2011; Zhong et al., 2016). All four factors are highlighted with light yellow background in Table 1.

3.2.3. Neural stimulation pathways are prominently affected

Thus, specific pathways such as calcium homeostasis, GTP-binding regulators, membrane-associated ATPases, endocytosis, protein turnover modulators and energy metabolism appeared as recurrent functions among the known and potential Parkin substrates (see Fig. 1). For an unbiased investigation of such clustering, we performed a formal bioinformatics enrichment assessment of GO terms, KEGG pathways and Pfam domains among all documented > 2 fold ubiquitylation changes in Table 1 at the STRING website (all results with ranking are shown in several datasheets of Supplementary Table 1), hoping to gain insight into mitochondrial and extra-mitochondrial effects of Parkin.

3.3. Evidently reduced ubiquitination of other factors in the ubiquitin/protein degradation pathways

3.3.1. Bioinformatic enrichment of protein degradation factors within ubiquitylome profile

Among the > 2-fold downregulations, enrichments of the GO Biological Process terms “modification-dependent protein catabolic process” (false discovery rate FDR = 0.001), of “ubiquitin-dependent protein catabolic processes” (FDR = 0.003) and of proteolysis (FDR = 0.005) seemed obviously relevant. This pathway was also enriched among the GO terms Molecular Function. The affected molecules included prominently the ubiquitin E3 ligase subunit DDB1 (−3.7-fold at amino acid §1121), which modulates G-protein coupled receptor turnover and may associate with the COP9 signalosome during responses to abnormal DNA (Cavadini et al., 2016; Li et al., 2018). It is interesting to note that an excessive ubiquitylation of the signalosome component COPS3 (+2.6-fold) was also observed.

3.3.2. Strong affection of EGFR and NF-kB turnover regulators

An almost as strong reduction of ubiquitylation was documented for the beta-catenin modulator, DNA-damage-response factor and NF-kB repressor USP34 (−3.2-fold) (Lui et al., 2011; Poalas et al., 2013; Sy et al., 2013), to similar extent as the EGFR-endocytosis regulator and NF-kB repressor CCDC50 (−3.4 at §152 and − 2.0 at §129) that contains several ubiquitin-interactor domains (Bohgaki et al., 2008; Tashiro et al., 2006; Tsukiyama et al., 2012). In this context, it is noteworthy that the EGFR-endocytosis repressor ANKRD13A (+3.2-fold at §217) and the CUL1-associated SCF complex subunit SKP1A (+2.3-fold at §56/57) were excessively ubiquitylated.

3.3.3. Moderate affection of two PD pathogenesis factors

Weaker reductions of ubiquitylation were observed for CUL5 (−2.7-fold) as component of E3 ubiquitin-protein ligase complexes, also named Vasopressin-Activated Calcium-Mobilizing Receptor, shown to act as SOCS6-associated repressor of Src/Cas-dependent membrane dynamics and autophagy (Antonioli et al., 2014; Teckchandani et al., 2014); the same extent was also observed for the ubiquitin hydrolase UCHL1 (−2.7-fold), which was also named PARK5 since missense mutations were observed in a family with hereditary Parkinson's disease (Leroy et al., 1998); for the proteasome subunit PSMA2 (−2.5-fold), which serves as selective target of the SCF ubiquitin E3 ligase complex containing FBXO7, also named PARK15 because of mutations associated with Parkinson's disease (Vingill et al., 2016); finally similar effects were documented for the peptide turnover enzyme DNPEP (−2.5-fold) and NPEPPS (−2.2-fold) as a synaptic protease (Huber et al., 1999).

3.3.4. Weak affection of other growth/stress regulators

Small effect sizes were found for the hepatocyte growth factor-regulated tyrosine kinase substrate and ubiquitin-interactor HGS (−2.3-fold) (Katz et al., 2002), for the ubiquitin-activating E1 enzyme UBA1 (−2.1-fold), and the Parkin-homologous cullin-RING ubiquitin ligase complex-associated ARIH1 (−2.0-fold) that triggers translation arrest in response to DNA-damage (Aguilera et al., 2000; von Stechow et al., 2015).

In summary, several dysregulated factors within the protein turnover pathways are known modulators of endocytotic internalization and inflammatory responses to abnormal DNA. These findings provide a molecular basis, which may explain a recent report that Parkin controls metazoan innate immune defense against bacteria, via modulation of phagocytic uptake and inflammatory responses (Manzanillo et al., 2013).

3.4. Bioinformatic assessment of pathway enrichments points to prominent vesicle pathology and cGMP/calcium dependent signaling

3.4.1. Decreased ubiquitylation

Among the downregulations, the unbiased bioinformatics assessment observed a prominent enrichment for “vesicles” with an outstanding number of 48 factors showing dysregulation within the GO terms for Cellular Components (Supplementary Table 1; illustrated as red bullets in Fig. 2A), prominent enrichments for “gastric acid secretion”, “cGMP-PKG signaling pathway”, “endocrine and other factor-regulated calcium reabsorption” and “cardiac muscle contraction” within the KEGG pathways were mainly based on the same factors (ATP-driven channels).

3.4.2. Increased ubiquitylation

Among the upregulations, prominent enrichments were found for “cellular ion homeostasis” and “regulation of membrane potential” among the GO terms Biological Processes, for “anion binding” among the GO terms Molecular Functions, for “membrane-bounded vesicles” among the GO terms Cellular Components (illustrated as purple bullets in Fig. 2B), for “cGMP-PKG signaling pathway” and “calcium signaling” among the KEGG pathways (Supplementary Table 1).

3.4.3. Enrichment of calcium signaling factors

Beyond the bioinformatically defined pathway components, the importance of calcium homeostasis was also emphasized by the striking upregulation of the Golgi-associated calcium pump ATP2C1 (§8 + 7.2-fold) and of the Amyloid Beta A4 precursor APP (§688/728/763 + 4.7-fold), which is a known modulator of calcium currents during multiple challenges with nicotine or caffeine via sensitization or overfilling of endoplasmic reticulum stores that are maintained by SERCA (ATP2A) pump and mitochondrial calcium efflux (Chin et al., 2006). Further support came from the downregulations of the calcium-regulated actin assembly promoter GSN (§317/366–2.1-fold), the calcium oscillation generator GNPDA1 (§197–2.0-fold), the calcium-dependent synaptic vesicle interactor SYT2 (§115–2.0-fold), and the calcium-dependent interactor with ER/plasma membranes ESYT1 (§339–2.0-fold). Most importantly, the calcium signaling pathway had already been highlighted by the strong ubiquitylation deficits of Hippocalcin and Calmodulin, marked with purple background in Table 1. Hippocalcin is a neuron-specific Ca^{2+}-sensor, which modulates the pool of cyclic GMP that is catalyzed by the membrane bound guanylate cyclase transduction system (Krishnan et al., 2009) and which was also found to regulate voltage-dependent calcium channels (Helassa et al., 2017). During axonal signal transduction, Hippocalcin gates the calcium activation of KCNQ-dependent potassium currents that mediate the slow after-hyperpolarization (sAHP), which follow any train of action potentials (Kim et al., 2016b; Kim et al., 2012; Tzingounis et al., 2007). Deficiency of Hippocalcin does not lead to adaptation of expression in other neural calcium-sensors such as VILIP-1 / VILIP-3 / NCS-1 (Kobayashi et al.,

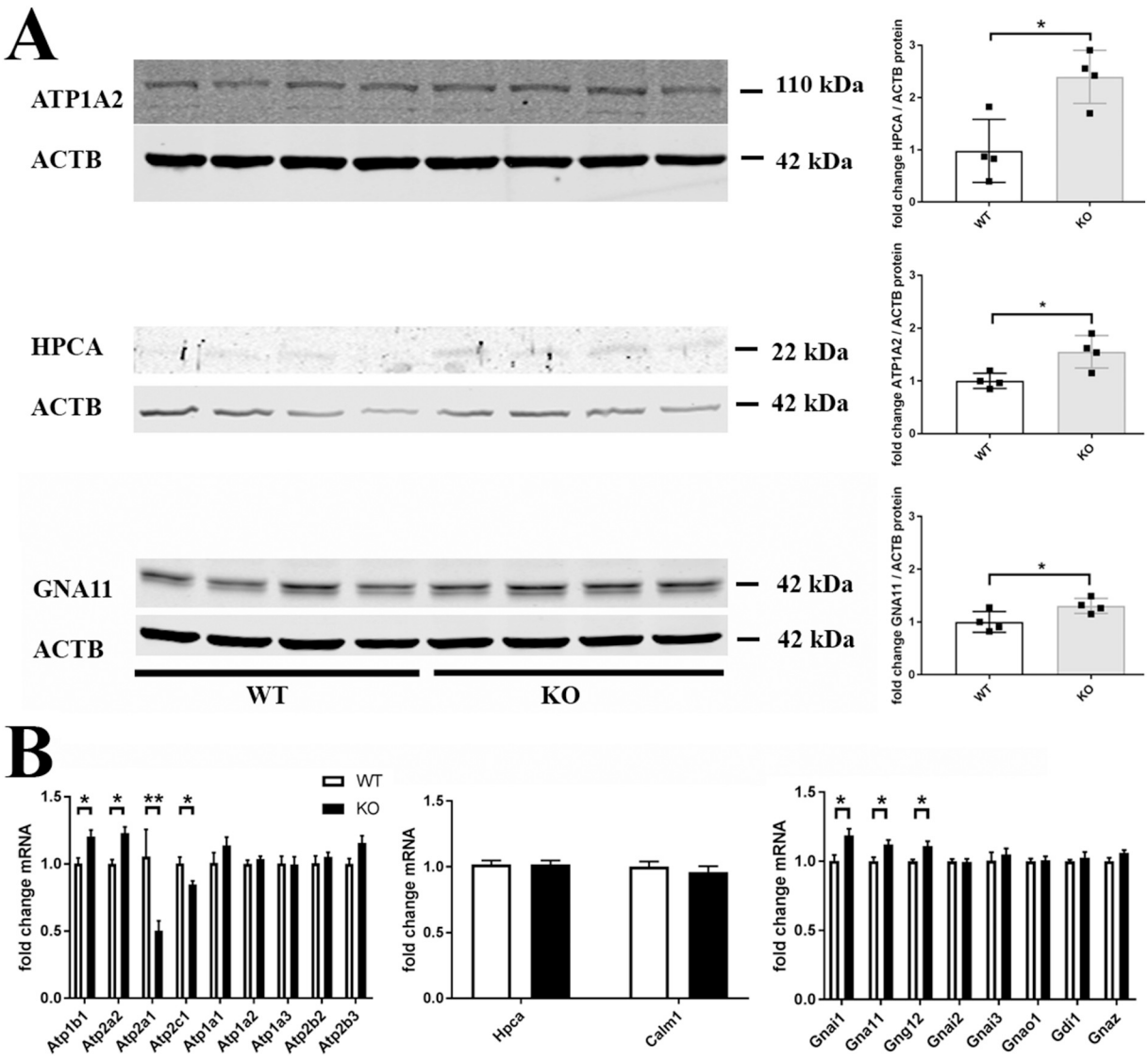

Fig. 3. Validation by analyses of steady-state expression levels in brain tissues from 18-month-old mice. (A) Protein: Quantitative immunoblots showed Hippocalcin and GNA11 to be significantly increased in the RIPA fraction, and ATP1A2 significantly increased in the SDS fraction, while VDAC in the SDS fraction as well as Gα(i) in the RIPA fraction appeared unchanged (data not shown) (n = 4 wildtype vs. 4 mutant mice). Significance was determined with unpaired Student's t-test and illustrated in the bar graphs by asterisks (* = $p < .05$). **(B)** mRNA: Quantitative reverse transcriptase PCR demonstrated significantly elevated mRNA levels for the ATP-driven ion channels *Atp1b1* and *Atp2a2*, while the expression levels of *Atp2a1* and *Atp2c1* were reduced. The transcript levels of *Hpca* and *Calm1* appeared unchanged. Levels of the G-protein subunits *Gnai1* and *Gna11 and Gng12* were significantly increased (n = 4 wildtype vs. 4 mutant mice). Significance was determined with unpaired Student's t-test and illustrated in the bar graphs by asterisks (* = $p < .05$, ** = $p < .01$).

2005), but it is unknown whether it triggers compensatory changes in G-protein subunit expression.

3.4.4. Additional enrichment of calcium-dependent after hyperpolarization factors

Thus, it appears meaningful that PRMT1 showed decreased ubiquitylation (§314/324/342–2.3-fold), as a modulator of the Hippocalcin interactor KCNQ (Kim et al., 2016a; Kim et al., 2012), similar to the calcium channel interactor and endocytosis regulator DPYSL2 (CRMP2, −3.5-fold at §423, −2.5-fold at §146), which controls the surface transport of KCNQ (Jiang et al., 2015). Further support for the relevance of afterhyperpolarization comes from the observation that HCN2 shows an excessive ubiquitylation (+2.0-fold at §510), as a hyperpolarization-activated and cyclic-nucleotide-gated potassium and sodium channel (Ingram and Williams, 1996) that has important pacemaker modifying roles in neurons and heart. HCN contributes to afterhyperpolarization and modulates dopaminergic (D2) modulation of the sAHP in striatal neurons (Deng et al., 2007; Gu et al., 2005). Additional findings are consistent with this context, in particular the excessive ubiquitylation of a peptide from the voltage-gated calcium channel CACNA1B (+2.1-fold at §65) and other calcium and sodium pumps (ATP2C1 §8 + 7.2-fold, ATP1A1 §177 + 2.2-fold, ATP2B2 §191 + 2.2-fold, ATP2A2 §628 + 2.1-fold, but ATP1A1 §36/37–2.0-fold, ATP1B1 §5–2.0-fold, ATP1A2 §505–2.3-fold, ATP1A1/ATP1A3/ATP1A4 §162/152/172–3.8-fold), some of which are also known modulators of sAHP (Tiwari et al., 2018). Overall, this combined evidence led us to focus on functional tests of axonal slow after-hyperpolarization and action potential firing frequency.

3.4.5. Enrichment of cGMP-PKG signaling, GTPases, G-proteins

This enrichment involved not only the factors recognized by bioinformatics and listed in Supplementary Table 1, namely ATP1A1, ATP1A2, ATP1B1, CALM1, GNAI1, PPP3CA, but also the Rab27A-GTPase activating protein alpha (TBC1D10A §99/100–3.7-fold), the

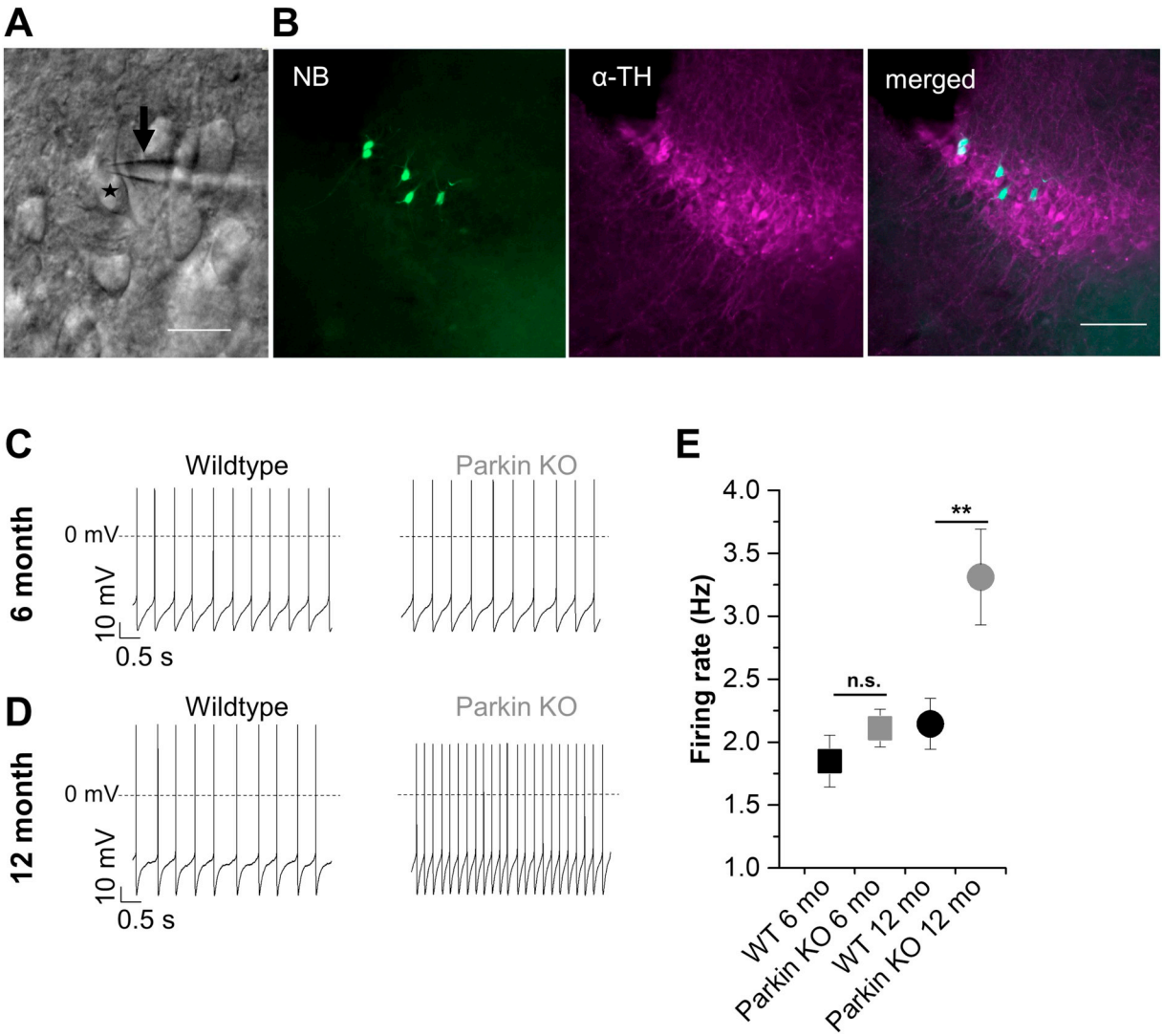

Fig. 4. Analysis of the intrinsic firing patterns of WT and Parkin-KO noradrenergic LC neurons. (A) Representative image of a patch pipette (black arrow) approaching a LC neuron (asterisk). Scale bar: 20 µm. **(B)** Co-staining of neurobiotin (NB) filled neurons with Alexa488 conjugated streptavidin (green) and anti-TH/anti-rabbit Alexa568 (magenta). Scale bar: 200 µm. **(C-D)** Example recordings of a spontaneously active WT (black) and Parkin-KO (grey) LC neuron from 6-month-old (upper panel) or 12-month-old (lower panel) mice in the whole-cell current clamp configuration. To isolate autonomous spiking, GABAergic (CGP, gabazine) and glutamatergic (AP-5, NBQX) blockers were added to the bath solution (ACSF). **(E)** Quantification of the firing rate revealed a significantly higher action potential frequency in the Parkin-KO group at the age of 12 months (WT 6 months: 1.85 ± 0.20 Hz, $n = 24$; Parkin-KO 6 months: 2.11 ± 0.15 Hz, $n = 34$; WT 12 months: 2.14 ± 0.20 Hz, $n = 20$; Parkin-KO 12 months: 3.31 ± 0.38 Hz, $n = 16$). Data are presented as mean ± S.E.M.; n.s.: not significant; **: $p < .01$ using unpaired Student's *t*-test, as these data followed a normal distribution. (For interpretation of the references to colour in this figure legend, the reader is referred to the web version of this article.)

Smoothened G-protein coupled receptor modulator DDB1 (§1121–3.7-fold), the Rab GDP-dissociation inhibitor GDI1 (§435–2.3-fold), the G-protein coupled receptor responsiveness modulator EFR3B (§595/639–2.2-fold), the Rho GDP-dissociation inhibitor ARHGDIA (§141–2.0-fold), the G protein subunit GNG12 (§34–2.0-fold), the RAB3A interactor RPH3A (§84 + 2.2-fold), the RP2 RabGAP interactor CFAP36 (§116 + 2.8-fold) and interestingly also the Amyloid Beta A4 precursor APP (§688/728/763 + 4.7-fold), which inhibits G(o) alpha ATPase activity (Ramaker et al., 2013). The known role of Parkin for the mitochondrial GTPases MFN1 and DRP1, the novel strong dysregulation of the neural cGMP modulator Hippocalcin and this additional cGMP-PKG signaling pathway enrichment in old Parkin-KO brain made us conduct a systematic assessment of G-protein subunit expression.

3.5. Molecular validation by analyses of steady-state expression

We attempted to elucidate if (1) the ubiquitylation changes influence the steady-state levels of the respective proteins, (2) they are accompanied by compensatory or additive adaptations of mRNA expression, and (3) they trigger homeostatic responses among other pathway components. Given that the ubiquitylome profile (Table 1) quantified peptides from several protein families where dysregulation may reflect only a specific isoform, validation with different approaches was necessary to identify the underlying factors. For this purpose, quantitative immunoblots and RT-qPCR were used in extracts from independent brains. A few commercial antibodies showed sufficient sensitivity and specificity to quantify independent epitopes in the endogenous levels of such proteins against whole brain background. In contrast, for the transcripts of almost all isoforms there were specific commercial assays at the RT-qPCR level. The experiments were focused on the families of ATP-driven Ca^{2+} pumps and Na^{+}/K^{+} pumps, Hippocalcin and Calmodulin as well as the G-protein subunits, as novel findings that are important for neural excitation.

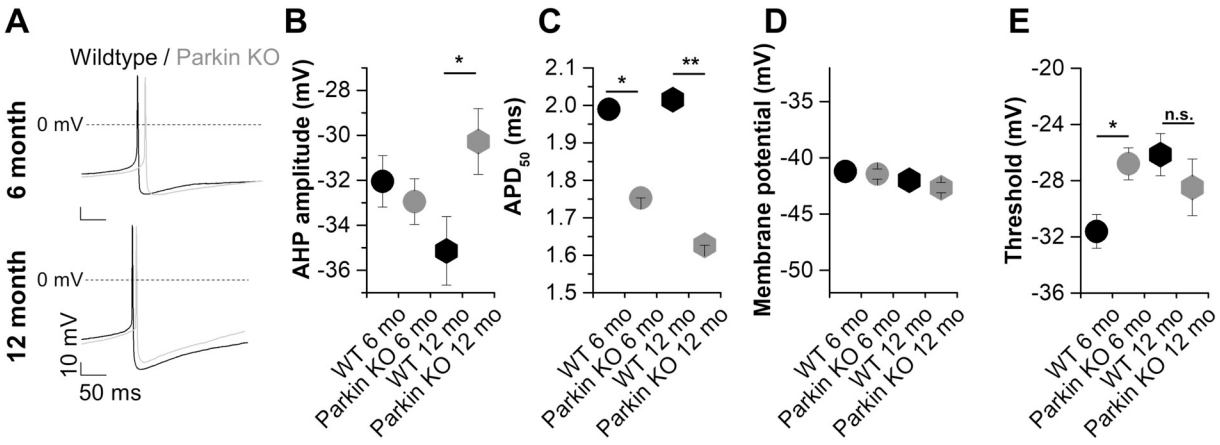

Fig. 5. Analysis of action potential parameters of WT and Parkin-KO LC neurons. (A) Overlay of representative current clamp recordings of WT (black) and Parkin-KO (grey) LC neurons of 6-month-old (upper panel) or 12-month-old (lower panel) mice. **(B)** Quantification of the afterhyperpolarization (AHP) amplitude revealed a significant decrease in Parkin-KO neurons at the age of 12 months (WT 6 months: −32.05 ± 1.14 mV; Parkin-KO 6 months: −32.95 ± 1.01 mV; WT 12 months: −35.14 ± 1.52 mV; Parkin-KO 12 months: −30.28 ± 1.46 mV). AHP amplitude was defined as the differential between the AP threshold and the most negative potential and AP threshold was defined as the membrane voltage at which APs at high resolution illustrate an abrupt rise. **(C)** Action potential duration (APD_{50}) was reduced in Parkin-KO neurons of mice at the age of 6 and 12 months (WT 6 months: 1.99 ± 0.09 ms; Parkin-KO 6 months: 1.75 ± 0.06 ms; WT 12 months: 2.02 ± 0.09 ms; Parkin-KO 12 months: 1.63 ± 0.08). No differences were observed concerning the mean membrane potential (WT 6 months: −41.21 ± 0.81 mV; Parkin-KO 6 months: −41.44 ± 0.46 mV; WT 12 months: −42.00 ± 0.61 mV; Parkin-KO 12 months: −42.67 ± 0.44 mV) **(D)** and the action potential threshold (WT 6 months: −31.62 ± 1.19 mV; Parkin-KO 6 months: −26.80 ± 1.13 mV; WT 12 months: −26.15 ± 1.51 mV; Parkin-KO 12 months: −28.48 ± 2.01 mV) **(E)**. (B-E: WT 6 months, $n = 19$; Parkin-KO 6 months, $n = 35$; WT 12 months, n = 20; Parkin-KO 12 months, $n = 15$). Data are presented as mean ± S.E.M. *: $p < .05$; **: $p < .01$ using unpaired Student's t-test, as these data followed a normal distribution.

3.5.1. At the protein level

Upon analysis of the steady-state of protein abundance, significantly increased abundance was confirmed (see Fig. 3A) for ATP1A2 (1.55-fold, $p = .018$), for Hippocalcin (2.4-fold, $p = .011$) and for GNA11 (1.3-fold, $p = .045$), a key mediator of membrane currents and action potentials in response to extracellular calcium, which can trigger hypocalcemia (Nesbit et al., 2013; Pahlavan et al., 2012; Roszko et al., 2017). In contrast, the levels of the mitochondrial voltage-gated anion channels Porin and the inhibitory G-protein subunit Gα(i) appeared unchanged. Unfortunately, an antibody that targets VDAC3 selectively is not available, the employed anti-Porin antibody recognizes VDAC1–3, with VDAC1 as the most abundant and VDAC3 being the least abundant isoform. Thus, the increased level of VDAC3 protein could not be demonstrated.

3.5.2. At the mRNA level

Significantly altered expression was documented (see Fig. 3B) for the ATP-driven Ca^{2+} pumps *Atp2a1* (0.50-fold, p = .04), *Atp2a2* (1.23-fold, $p = .003$), *Atp2c1* (0.85-fold, $p = .03$) and the ATP-driven Na^+/K^+ pump *Atp1b1* (1.20-fold, p = .01), as well as the G-protein subunits *Gnai1* (1.19-fold, p = .01), *Gna11* (1.12-fold, $p = .02$) and *Gng12* (1.11-fold, p = .02), while the transcripts for the calcium-sensors *Hpca* and *Calm1,* as well as the transcripts for the ion pump *Atp1a2* appeared normal. The dysregulation of the endoplasmic reticulum associated SERCA isoforms (*Atp2a1* and *Atp2a2*) appeared prominent; they play a role in the axon initial segment for the generation of axon potentials (Anton-Fernandez et al., 2015; Zhao et al., 2001) and interact with mitochondrial calcium pumps (Surmeier et al., 2012).

3.5.3. Is increased abundance of GNA11, HPCA and ATP1A2 protein due to turnover or re-synthesis?

The above findings document that selected factors within pathways of neural signaling and excitability show not only ubiquitylation changes, but also altered protein abundance and/or mRNA expression. Upon synopsis of all data it is usually impossible to predict which changes constitute primary mutation effects with pathogenic consequences, or which other events are homeostatic responses. In the case of the inhibitory G-protein subunit GNAI1 it is clear that its +5.4-fold elevated ubiquitylation at §47/51 would decrease its protein steady-state levels, but its −2.2-fold reduced ubiquitylation at §330/31 and its increased mRNA levels would oppose this effect, acting to maintain the normal GNAI1 levels that were observed experimentally upon quantitative immunoblotting. In the case of the phospholipase C activating subunit GNA11, significantly elevated protein levels were documented and appear to be due to a transcriptional upregulation effort. Regarding HPCA in contrast, its increased protein levels appear to be caused by the decreased protein degradation (the −4.7-fold decrease of ubiquitylation at §137) in view of its unchanged mRNA expression, and would act to enhance slow afterhyperpolarization after axonal action potentials. It is not clear whether this dysregulation is a pathological or a compensatory event. Considering ATP1A2, its elevated protein levels seem to be simply due to decreased ubiquitylation (−2.3-fold at §505) in view of its unchanged mRNA expression. Thus, both Hippocalcin and ATP1A2 might represent novel Parkin substrates.

3.6. Effects of Parkin-KO on neuronal electrophysiology

3.6.1. Focusing on brainstem noradrenergic signals

It remained unclear, which molecular changes represent primary pathology, which dysregulations are compensating a problem over some time, and how they progressively impair neural function. It was previously reported that these mice show discrete deficits of hippocampal long-term potentiation, spatial memory and open-field habituation (Rial et al., 2014). To elucidate these questions further, we undertook the laborious assessment of electrophysiology of activation pathways in acute brain slices. In view of the previously reported preferential vulnerability of the brainstem locus coeruleus (LC) in Parkin-KO brains (Von Coelln et al., 2004), our work attempted to find maximal phenotypes, thus focusing on LC neurons that serve in noradrenergic G-protein coupled receptor signaling, rather than the midbrain dopaminergic substantia nigra (SN) neurons or hippocampus. To take homeostatic efforts at earlier ages versus manifestation of phenotypes at later ages into account, 6-month-old versus 12-month-old mutant and wildtype mice derived from the same ancestors and maintained in adjacent cages under identical conditions were assessed. To investigate axonal firing patterns in acute brainstem slices for

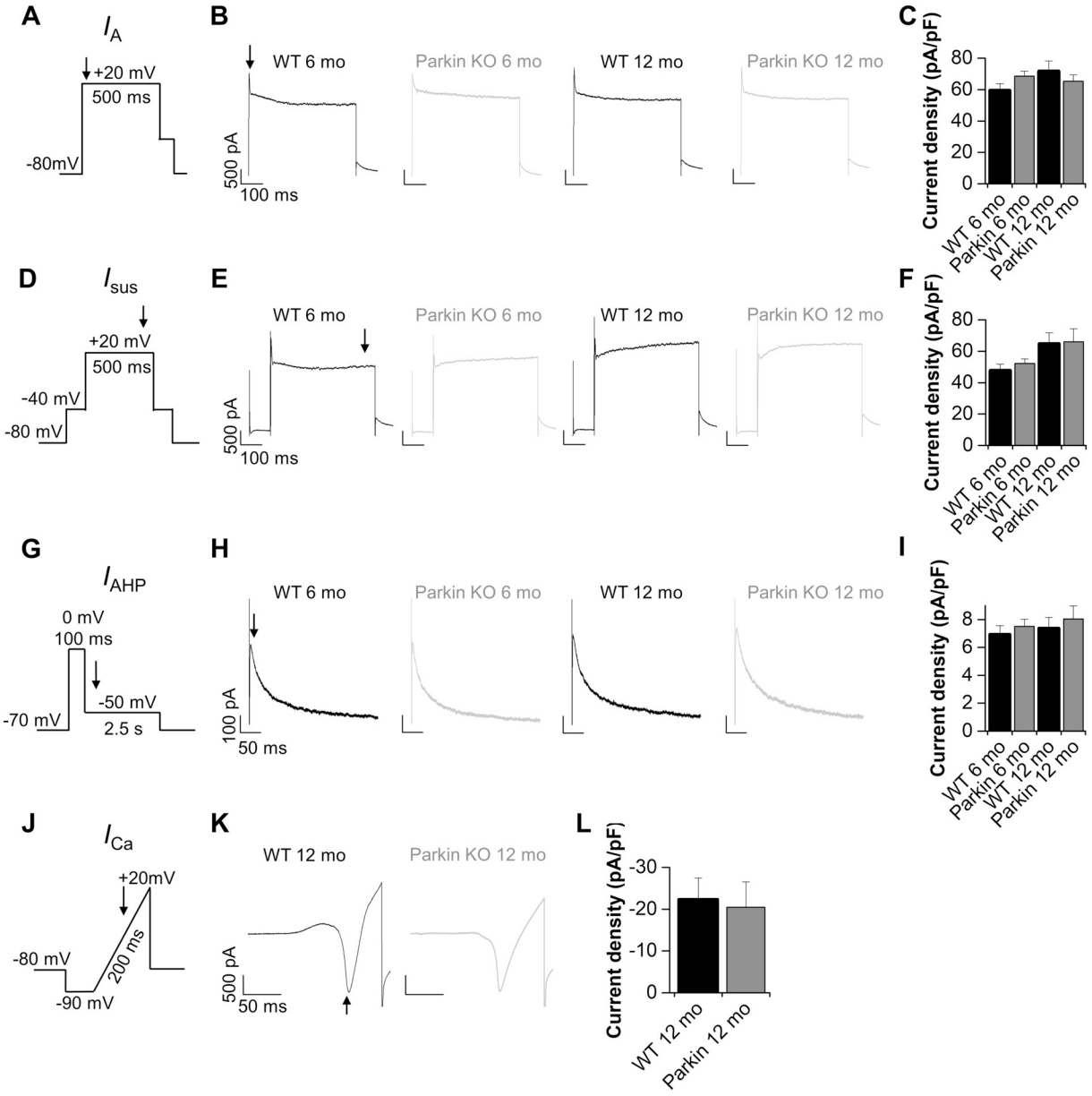

Fig. 6. Comparison of K^+ and Ca^{2+} currents in LC neurons of WT and Parkin-KO mice. (A-C) Analysis of the rapidly inactivating component of the K^+ outward current (I_A) at 20 mV obtained with the voltage step protocol depicted in **(A).** As indicated by arrows peak current was analyzed directly at the beginning of the voltage step to 20 mV. **(B)** Representative whole-cell voltage clamp recordings. **(C)** Quantification of I_A did not reveal any significant difference between the groups (WT 6 months: 59.43 ± 48 pA/pF, n = 17; Parkin-KO 6 months: 68.65 ± 3.23 pA/pF, n = 30; WT 12 months: 71.69 ± 6.58, n = 19; Parkin-KO 12 months: 65.28 ± 4.11 pA/pF, n = 21). **(D-F)** Analysis of the sustained component of the K^+ outward current (I_{sus}) at 20 mV obtained with a voltage step protocol comprising a pre-pulse to −40 mV as displayed in **(D).** **(E)** Representative whole-cell voltage clamp recordings. **(F)** Quantification of I_{sus} (WT 6 months: 47.70 ± 4.06 pA/pF, n = 17; Parkin-KO 6 months: 52.31 ± 2.80 pA/pF, n = 31; WT 12 months: 64.66 ± 7.13 pA/pF, n = 19; Parkin-KO 12 months: 66.10 ± 8.22 pA/pF, n = 21). **(G-I)** Analysis of the K^+ current flowing during the afterhyperpolarization (I_{AHP}). AHP currents were evoked by the two-step voltage protocol depicted in **(G)** and analyzed at the step to −50 mV. **(H)** Representative whole-cell voltage clamp recording of AHP currents. **(I)** Mean AHP current densities were: WT 6 months: 6.92 ± 0.66 pA/pF, n = 17; Parkin-KO 6 months: 7.51 ± 0.52 pA/pF, n = 30; WT 12 months: 7.35 ± 0.80 pA/pF, n = 17 and Parkin-KO 12 months: 8.05 ± 0.92 pA/pF, n = 19). **(J-L)** Analysis of peak Ca^{2+} inward currents obtained with the voltage ramp shown in **(J)** and using a cesium based internal solution. ACSF was complemented with 1 µM TTX. **(K)** Representative whole-cell voltage clamp recording of Ca^{2+} inward currents. **(L)** Analysis of peak Ca^{2+} inward currents did not reveal a significant difference between WT and Parkin-KO (WT 12 months: −22.26 ± 5.23 pA/pF, n = 4; Parkin-KO 12 months: −20.43 ± 6.07 pA/pF, n = 5). Data are presented as mean ± S.E.M.

murine LC neurons, which were histologically verified as previously described (Henrich et al., 2018; Matschke et al., 2015; Matschke et al., 2018) (Fig. 4A-B), whole-cell current clamp and voltage clamp experiments were conducted (Figs. 4–7).

3.6.2. Progressive alteration of the intrinsic pacemaking frequency

The intrinsic firing pattern of LC neurons recorded in the whole cell current clamp mode showed a significantly higher action potential frequency in Parkin-KO mice at the age of 12 months (Fig. 4C-E). In parallel, the afterhyperpolarization (AHP) amplitude was significantly decreased at this age (Fig. 5A-B), an interesting finding in view of the influence of Hippocalcin on sAHP (Kim et al., 2012; Larsson, 2013; Tzingounis et al., 2007). Already at the age of 6 months and again at 12 months, the action potential duration (APD_{50}) was significantly

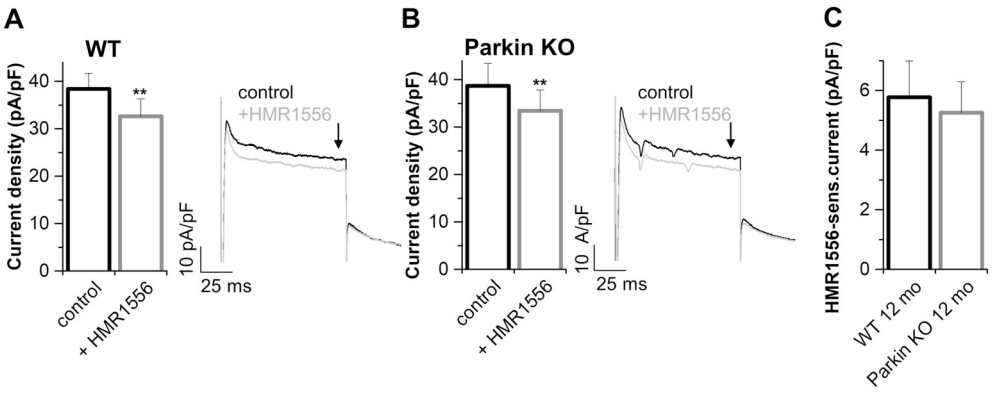

Fig. 7. Analysis of KCNQ mediated currents in LC neurons of 12-month-old WT and Parkin-KO mice. It is known that the calcium buffer protein Hippocalcin, which shows an altered turnover in Parkin-KO mice, interacts with the Ca^{2+} sensor of KCNQ channels, thereby modulating the slow AHP current (Kim et al., 2012). We therefore tested whether KCNQ mediated currents are altered in 12-month-old Parkin-KO mice using the KCNQ channel blocker HMR1556. Currents were evoked with the same voltage clamp protocol as shown in Fig. 6 D. **(A-B)** Analysis of sustained K^+ outward currents (left panels) and sample traces of evoked currents (right panels) of WT **(A)** and Parkin-KO **(B)** LC neurons at 0 mV before (control) and after wash in of 1 µM HMR1556. In both groups drug application induced a significant decrease of the K^+ outward current (WT control: 38.38 ± 3.26 pA/pF, $n = 6$; WT + HMR1556: 32.61 ± 3.70 pA/pF, n = 6; Parkin-KO control: 38.71 ± 4.73 pA7pF, $n = 7$; Parkin-KO + HMR1556: 33.45 ± 4.35 pA/pF, n = 7). **(C)** Comparison of the HMR1556 sensitive current did not reveal a significant difference between WT and Parkin-KO mice (WT 12 months: 5.77 ± 1.22 pA/pF; Parkin-KO 12 months: 5.26 ± 1.04 pA/pF). Data are presented as mean ± S.E.M. **: $p < .01$ using unpaired Student's t-test, as these data followed a normal distribution.

reduced (Fig. 5C), while the mean membrane potential and the action potential threshold appeared normal (Fig. 5D-E).

3.6.3. Underlying mechanism not explained by distinct changes in ionic currents across the plasma membrane

To investigate whether the altered firing behavior of aged Parkin-KO LC neurons is reflected by changes of distinct ionic conductances, we subsequently used different voltage clamp protocols to isolate K^+ and Ca^{2+} currents across the plasma membrane. The study of the I_A (Fig. 6A-C) and I_{sus} (Fig. 6D-F) K^+ currents revealed no significant differences in macroscopic potassium flux in Parkin-KO LC neurons, both, at the age of 6 and 12 months. Also the I_{AHP} (Fig. 6G-I) and the Ca^{2+} currents (Fig. 6J-L) regulating the afterhyperpolarization in LC neurons (Matschke et al., 2018) were not significantly altered in the LC neurons of Parkin-KO mice. Given that Hippocalcin is known to modulate sAHP via its interaction with the calcium sensor of KCNQ (Kim et al., 2012) and that the KCNQ-interactors PRMT1 and DPYSL2 showed decreased ubiquitylation, the KCNQ-specific antagonist HMR1556 was used to isolate KCNQ-mediated component of the I_{sus} current (Fig. 7A-C). However, we did not identify significantly different HMR1556-sensitive current components in 12-month-old Parkin-KO mice (Fig. 7C), suggesting that KCNQ channels are not functionally altered. Thus, the AHP amplitude is altered in Parkin-KO mice while in whole cell voltage-clamp recordings with a `clamped´ Ca^{2+} concentration, the I_{AHP} and Ca^{2+} currents are not altered. These negative findings are consistent with the concept that the alterations in AHP, APD_{50} and action potential frequency are consequences of anomalies in calcium homeostasis and other ion membrane pumps and not by altered expression levels or functional properties of K^+ or Ca^{2+} channels at the plasma membrane.

4. Discussion

To understand Parkin-dependent protein post-translational modifications in whole brain and their functional consequences in noradrenergic LC neurons, we undertook a global ubiquitylome survey and validation work by immunoblots, qPCR and electrophysiology. As expected, the strongest Parkin-dependent ubiquitylation deficit was observed for mitochondrial outer membrane protein VDAC3, providing proof-of-principle that our approach is consistent with previous work on peripheral tumor cell lines like HeLa. Several novel ubiquitylation deficits were identified in protein complexes and pathways that are under control of Parkin, so TBC1D10A, SIRT2, OTUD7B and CUL5 may represent direct Parkin targets, but this has to be assessed further in overexpression and co-immunoprecipitation experiments. In this manuscript, we maintained the focus on neuron-specific factors that influence axonal excitability, based on the bioinformatics enrichment of dysregulations among ion channels, calcium homeostasis and G-protein dependent signaling.

As a novel candidate Parkin substrate, ATP1A2 showed increased abundance due to reduced ubiquitylation at residue 505 in absence of transcriptional regulation. Relatively little is known about ATP1A2 in the nervous system. According to studies that relied on the monoclonal antibody McB2 (Cholet et al., 2002), at adult age the main brain expression of ATP1A2 occurs in astrocytes, but it may be important to note that adult mouse brain shows a predominant neural expression of *Atp1a2* mRNA according to the internet database Allen mouse brain atlas (http://mouse.brain-map.org/). ATP1A2 deficiency leads to reduced burst activity in neurons (Moseley et al., 2003) and modulates calcium dynamics (Despa et al., 2012; Hartford et al., 2004). Mutations in ATP1A2 trigger the pathogenesis of migraine in interaction with voltage-gated calcium channels (Lafreniere and Rouleau, 2011).

Hippocalcin is a Ca^{2+} sensor of a variant form of the ROS-GC subfamily of membrane guanylate cyclases that senses physiological increments of Ca^{2+} and stimulates ONE-GC membrane guanylate cyclase, controlling about 30% of the total membrane guanylate cyclase transduction system (Krishnan et al., 2009). In this way, it modulates G-protein coupled receptor signals and second messenger cascades (Mammen et al., 2004; Sallese et al., 2000). Its mRNA is expressed strongly in pyramidal cells of the hippocampus and in Purkinje neurons of the cerebellum, but it is found also in cerebral cortex neurons and in large neurons of the striatum (Saitoh et al., 1993). It appears to be particularly crucial for the dopaminergic nigrostriatal projections, since its mutation triggers a phenotype of primary isolated dystonia, named DYT2 (Charlesworth et al., 2015). Its expression downregulation accompanies the onset of Huntington's disease, where striatal neurodegeneration with motor hyperactivity are the prominent features (Luthi-Carter et al., 2002; Luthi-Carter et al., 2000). Hippocalcin deficiency impairs the neuronal responses of calcium-dependent excitation to glutamate (Charlesworth et al., 2015). The interaction between muscarinic acetylcholine receptors and glutamatergic NMDA receptors in the control of long-term depression depends on Hippocalcin, so postsynaptic excitability is modulated by it (Amici et al., 2009; Jo et al., 2010; Palmer et al., 2005). Hippocalcin binds to brain-type creatine kinase and modulates its calcium-dependent translocation to membranes (Kobayashi et al., 2012). Importantly, it also binds to the neuronal apoptosis inhibitory protein (NAIP). The HPCA-NAIP complex protects neurons from mitochondrial dysfunction, counteracting pathological calcium release and caspase activation (Mercer et al., 2000). Diverse NAIP isoforms are crucial in eukaryotic cells for the detection of

invading bacterial proteins, activation of the inflammasome and of pyroptosis (Amarante-Mendes et al., 2018; Kofoed and Vance, 2011; Reyes Ruiz et al., 2017; Zhao et al., 2011). In the Parkin-KO mouse brain, we observed increased levels of Hippocalcin together with decreased ubiquitylation, a dysregulation that might be expected to enhance sAHP after axonal action potentials (Tzingounis et al., 2007). Our electrophysiological data, however, documented diminished sAHP in aged Parkin-KO. Thus, the reduced ubiquitylation of HPCA might not constitute a direct Parkin-KO effect, but rather an indirect compensatory neuronal effort to rescue the sAHP that is abnormally low due to the calcium dysregulations.

Although it was not identified as a target of Parkin-dependent ubiquitylation changes, GNA11 (Gα11) stands out for its selective transcriptional induction, which achieves a steady-state elevation of its protein levels. Gα11 does not permanently reside at plasma membranes, but can relocate to the outer mitochondrial membrane (in parallel to Gαq relocation to the mitochondrial inner membrane) where it is responsible for the proper equilibrium between fusion and fission (Beninca et al., 2014), which is maintained via altered levels of both mitofusin and Drp1 proteins. The GTPases mitofusin 1/2 and DRP1 are known as Parkin substrates, and in our study MFN1 showed reduced ubiquitylation in brain, therefore GTP turnover at the outer mitochondrial membrane might be altered. The absence of Gα11 was reported to decrease mitochondrial fusion rates and overall respiratory capacity, ATP production and OXPHOS-dependent growth (Beninca et al., 2014), so the induction of Gα11 in Parkin-KO brain might have the opposite neuroprotective effects. Importantly, Gα11 and Gαq modulate also Ca^{2+} release and Ca^{2+} entry in excitable cells (Macrez-Lepretre et al., 1997). At the same time, Gα11 and Gαq control neuronal excitability via the PLCβ signaling cascade and the calcium-sensitive, potassium-dependent afterhyperpolarizing current, which is modified by Hippocalcin and Neurocalcin delta (Krause et al., 2002; Madison and Nicoll, 1984; Pedarzani and Storm, 1993; Schwindt et al., 1988; Villalobos and Andrade, 2010). Thus, myocytes from the Gαq and/or Gα11 KO mice showed altered action potentials, membrane currents, and Ca^{2+} handling (Pahlavan et al., 2012). Cerebellar Purkinje and hippocampal pyramidal neurons from the Gαq and/or Gα11 KO mice showed altered synaptic plasticity and motor behavior (Hartmann et al., 2004; Miura et al., 2002). Therefore, the upregulation of Gα11 in Parkin-KO brain provides an interesting insight, how brain cells couple the mitochondrial function with calcium-dependent excitability and firing frequency regulation at the plasma membrane.

In conclusion, our pioneer study of the Parkin-KO brain ubiquitylome has identified several novel peptides and residues that show deficient posttranslational modifications. Two neuron-specific factors among them, ATP1A2 and Hippocalcin, show increased abundance in the absence of transcriptional activation. Both are known modulators of calcium-dependent action potential generation and afterhyperpolarization and indeed significant changes in these electrophysiological features were documented in noradrenergic LC neurons. Overall, the progressive changes in neuronal firing correlate well to the strong ubiquitylation decrease for several sodium/potassium-transporting ATPases (ATP1A1/2/3/4) and the strong ubiquitylation increase for ATP2C1 that sequestrates calcium to the secretion pathway (Brini et al., 2012). The increased neuronal excitability may also relate to the decreased ubiquitylation of protein kinase M (PKM), which was previously identified as possible Parkin substrate and which acts in calcium-dependent manner to induce burst firing in dopaminergic neurons (Liu et al., 2007; Sarraf et al., 2013). Interestingly, the action potential duration was already reduced at Parkin-KO ages of 6 months, whereas firing frequency and sAHP alterations were clearly abnormal only by 12 months of age. Investigations of the preferential vulnerability of brainstem and midbrain catecholaminergic neurons to Parkinsonian neurodegeneration have shown that they have an outstanding dependence of their pacemaker activity on L-type calcium channels at the plasma membrane (Matschke et al., 2015; Surmeier et al., 2012). The stimulus-dependent changes in their firing frequency require calcium homeostasis changes at mitochondria and endoplasmic reticulum, and it has been reported already that Parkin-deficiency may impair mitochondrial Ca^{2+} transients (Cali et al., 2014). It is also known that the degeneration of dopaminergic neurons in *Pink1*$^{-/-}$ zebrafish can be rescued by inhibition of the mitochondrial calcium-uptake uniporter MCU (Soman et al., 2017). The increased excitability and altered afterhyperpolarization due to altered mitochondrial Ca^{2+} homeostasis, which we observed in Parkin-KO mice, appear to be common features in PD animal models. Similar findings were made in mice with *Pink1*$^{-/-}$ genotypes (Bishop et al., 2010; Huang et al., 2017), where a strong transcriptional downregulation was observed for *Cisd2* as a factor that drives calcium transport from mitochondria to the endoplasmic reticulum (Gispert et al., 2015; Rouzier et al., 2017; Shen et al., 2017). Furthermore, mice with A53T-alpha-synuclein overexpression show increased firing frequencies in dopaminergic SN neurons, and mice with exposure to Parkinson-inducing drugs exhibit degeneration of dopaminergic SN neurons in dependence on mitochondrial K-ATP channels (Liss et al., 2005; Subramaniam et al., 2014). It is important to note that several drugs are now available that modulate the activity of mitochondrial VDAC, and that the drug isradipine protects dopaminergic SN neurons via modulation of mitochondrial dynamics and L-type calcium channels (Ben-Hail et al., 2016; Guzman et al., 2018). Future analyses are needed to distinguish direct from indirect Parkin effects, and understand why initial compensatory efforts lose their efficiency during brain ageing. Given that presymptomatic homozygous and compound heterozygous Parkin mutation carriers exhibit an increased frequency of depression (Reetz et al., 2008; Srivastava et al., 2011), and that *PARK2* gene microduplications were identified in attention-deficit/hyperactivity disorder (ADHD) patients (Dalla Vecchia et al., 2019), we believe that the mechanisms of Parkin-dependent neural excitability have wide clinical relevance.

Supplementary data to this article can be found online at https://doi.org/10.1016/j.nbd.2019.02.008.

Acknowledgements

We thank Birgitt Meseck-Selchow and Gabriele Köpf for technical assistance, and the animal care team at the ZFE Frankfurt (in particular the veterinarians Dr. Alf Theisen and Dr. Christa Tandi, as well as the caretakers Eleonora Daut and Birgit Janton). The study was financed with funds of the University Hospitals in Frankfurt and Marburg, and by the German Ministry of Health with the National Genome Research Network (NGFNplus, BMBF 01GS08138) and the GerontoMitoSys Network (BMBF PTJ 0315584A), and by the European Union through ERAnet-RePARK (DLR 01EW1012).

Competing interests

The authors declare that there is no competing interest regarding the publication of this manuscript.

References

Aguilera, M., et al., 2000. Ariadne-1: a vital Drosophila gene is required in development and defines a new conserved family of ring-finger proteins. Genetics 155, 1231–1244.
Amarante-Mendes, G.P., et al., 2018. Pattern recognition receptors and the host cell death molecular machinery. Front. Immunol. 9, 2379.
Amici, M., et al., 2009. Neuronal calcium sensors and synaptic plasticity. Biochem. Soc. Trans. 37, 1359–1363.
Anton-Fernandez, A., et al., 2015. Selective presence of a giant saccular organelle in the axon initial segment of a subpopulation of layer V pyramidal neurons. Brain Struct. Funct. 220, 869–884.
Antonioli, M., et al., 2014. AMBRA1 interplay with cullin E3 ubiquitin ligases regulates autophagy dynamics. Dev. Cell 31, 734–746.
Azarashvili, T., et al., 2009. Ca2+-dependent permeability transition regulation in rat brain mitochondria by 2′,3′-cyclic nucleotides and 2′,3′-cyclic nucleotide 3′-phosphodiesterase. Am. J. Phys. Cell Phys. 296, C1428–C1439.

Ben-Hail, D., et al., 2016. Novel compounds targeting the mitochondrial protein VDAC1 inhibit apoptosis and protect against mitochondrial dysfunction. J. Biol. Chem. 291, 24986–25003.
Beninca, C., et al., 2014. A new non-canonical pathway of Galpha(q) protein regulating mitochondrial dynamics and bioenergetics. Cell. Signal. 26, 1135–1146.
Bertolin, G., et al., 2013. The TOMM machinery is a molecular switch in PINK1 and PARK2/PARKIN-dependent mitochondrial clearance. Autophagy 9, 1801–1817.
Birsa, N., et al., 2014. Lysine 27 ubiquitination of the mitochondrial transport protein Miro is dependent on serine 65 of the parkin ubiquitin ligase. J. Biol. Chem. 289, 14569–14582.
Bishop, M.W., et al., 2010. Hyperexcitable substantia nigra dopamine neurons in PINK1- and HtrA2/Omi-deficient mice. J. Neurophysiol. 104, 3009–3020.
Bohgaki, M., et al., 2008. Involvement of Ymer in suppression of NF-kappaB activation by regulated interaction with lysine-63-linked polyubiquitin chain. Biochim. Biophys. Acta 1783, 826–837.
Brini, M., et al., 2012. Calcium pumps: why so many? Comprehensive Physiol. 2, 1045–1060.
Cali, T., et al., 2014. Calcium signaling in Parkinson's disease. Cell Tissue Res. 357, 439–454.
Carron, R., et al., 2014. Early hypersynchrony in juvenile PINK1(-)/(-) motor cortex is rescued by antidromic stimulation. Front. Syst. Neurosci. 8, 95.
Cavadini, S., et al., 2016. Cullin-RING ubiquitin E3 ligase regulation by the COP9 signalosome. Nature 531, 598–603.
Charlesworth, G., et al., 2015. Mutations in HPCA cause autosomal-recessive primary isolated dystonia. Am. J. Hum. Genet. 96, 657–665.
Chin, J.H., et al., 2006. Beta-amyloid enhances intracellular calcium rises mediated by repeated activation of intracellular calcium stores and nicotinic receptors in acutely dissociated rat basal forebrain neurons. Brain Cell Biol. 35, 173–186.
Cholet, N., et al., 2002. Similar perisynaptic glial localization for the Na+,K+-ATPase alpha 2 subunit and the glutamate transporters GLAST and GLT-1 in the rat somatosensory cortex. Cereb. Cortex 12, 515–525.
Corti, O., et al., 2011. What genetics tells us about the causes and mechanisms of Parkinson's disease. Physiol. Rev. 91, 1161–1218.
Dalla Vecchia, E., et al., 2019. Cross-species models of attention-deficit/hyperactivity disorder and autism spectrum disorder: lessons from CNTNAP2, ADGRL3, and PARK2. Psychiatr. Genet. 29, 1–17.
Dehorter, N., et al., 2012. Subthalamic lesion or levodopa treatment rescues giant GABAergic currents of PINK1-deficient striatum. J. Neurosci. 32, 18047–18053.
Deng, P., et al., 2007. Involvement of I(h) in dopamine modulation of tonic firing in striatal cholinergic interneurons. J. Neurosci. 27, 3148–3156.
Despa, S., et al., 2012. Na(+)/K(+)-ATPase alpha2-isoform preferentially modulates Ca2(+) transients and sarcoplasmic reticulum Ca2(+) release in cardiac myocytes. Cardiovasc. Res. 95, 480–486.
Fournier, M., et al., 2009. Parkin deficiency delays motor decline and disease manifestation in a mouse model of synucleinopathy. PLoS One 4, e6629.
Gautier, C.A., et al., 2016. The endoplasmic reticulum-mitochondria interface is perturbed in PARK2 knockout mice and patients with PARK2 mutations. Hum. Mol. Genet. 25, 2972–2984.
Gegg, M.E., et al., 2010. Mitofusin 1 and mitofusin 2 are ubiquitinated in a PINK1/parkin-dependent manner upon induction of mitophagy. Hum. Mol. Genet. 19, 4861–4870.
Gehrke, S., et al., 2015. PINK1 and parkin control localized translation of respiratory chain component mRNAs on mitochondria outer membrane. Cell Metab. 21, 95–108.
Geisler, S., et al., 2010. PINK1/parkin-mediated mitophagy is dependent on VDAC1 and p62/SQSTM1. Nat. Cell Biol. 12, 119–131.
Girirajan, S., et al., 2008. Tom1l2 hypomorphic mice exhibit increased incidence of infections and tumors and abnormal immunologic response. Mamm. Genome 19, 246–262.
Gispert, S., et al., 2009. Parkinson phenotype in aged PINK1-deficient mice is accompanied by progressive mitochondrial dysfunction in absence of neurodegeneration. PLoS One 4, e5777.
Gispert, S., et al., 2015. Potentiation of neurotoxicity in double-mutant mice with Pink1 ablation and A53T-SNCA overexpression. Hum. Mol. Genet. 24, 1061–1076.
Gu, N., et al., 2005. Kv7/KCNQ/M and HCN/h, but not KCa2/SK channels, contribute to the somatic medium after-hyperpolarization and excitability control in CA1 hippocampal pyramidal cells. J. Physiol. 566, 689–715.
Guzman, J.N., et al., 2018. Systemic isradipine treatment diminishes calcium-dependent mitochondrial oxidant stress. J. Clin. Invest. 128, 2266–2280.
Hammerling, B.C., et al., 2017a. A Rab5 endosomal pathway mediates parkin-dependent mitochondrial clearance. Nat. Commun. 8, 14050.
Hammerling, B.C., et al., 2017b. Isolation of Rab5-positive endosomes reveals a new mitochondrial degradation pathway utilized by BNIP3 and parkin. Small GTPases 1–8.
Hanson, J.E., et al., 2010. Altered hippocampal synaptic physiology in aged parkin-deficient mice. NeuroMolecular Med. 12, 270–276.
Hartford, A.K., et al., 2004. Na,K-ATPase alpha 2 inhibition alters calcium responses in optic nerve astrocytes. Glia 45, 229–237.
Hartmann, J., et al., 2004. Distinct roles of Galpha(q) and Galpha11 for Purkinje cell signaling and motor behavior. J. Neurosci. 24, 5119–5130.
Helassa, N., et al., 2017. Biophysical and functional characterization of hippocalcin mutants responsible for human dystonia. Hum. Mol. Genet. 26, 2426–2435.
Henrich, M.T., et al., 2018. A53T-alpha-synuclein overexpression in murine locus coeruleus induces Parkinson's disease-like pathology in neurons and glia. Acta Neuropathol. Commun. 6, 39.
Huang, E., et al., 2017. PINK1-mediated phosphorylation of LETM1 regulates mitochondrial calcium transport and protects neurons against mitochondrial stress. Nat. Commun. 8, 1399.
Huber, A.B., et al., 1999. Metalloprotease MP100: a synaptic protease in rat brain. Brain Res. 837, 193–202.
Imai, Y., Takahashi, R., 2004. How do Parkin mutations result in neurodegeneration? Curr. Opin. Neurobiol. 14, 384–389.
Ingram, S.L., Williams, J.T., 1996. Modulation of the hyperpolarization-activated current (Ih) by cyclic nucleotides in Guinea-pig primary afferent neurons. J. Physiol. 492, 97–106 Pt 1.
Itier, J.M., et al., 2003. Parkin gene inactivation alters behaviour and dopamine neurotransmission in the mouse. Hum. Mol. Genet. 12, 2277–2291.
Jiang, L., et al., 2015. Activation of m1 muscarinic acetylcholine receptor induces surface transport of KCNQ channels through a CRMP-2-mediated pathway. J. Cell Sci. 128, 4235–4245.
Jo, J., et al., 2010. Muscarinic receptors induce LTD of NMDAR EPSCs via a mechanism involving hippocalcin, AP2 and PSD-95. Nat. Neurosci. 13, 1216–1224.
Johnson, B.N., et al., 2012. The ubiquitin E3 ligase parkin regulates the proapoptotic function of Bax. Proc. Natl. Acad. Sci. U. S. A. 109, 6283–6288.
Katz, M., et al., 2002. Ligand-independent degradation of epidermal growth factor receptor involves receptor ubiquitylation and Hgs, an adaptor whose ubiquitin-interacting motif targets ubiquitylation by Nedd4. Traffic 3, 740–751.
Kim, W., et al., 2011. Systematic and quantitative assessment of the ubiquitin-modified proteome. Mol. Cell 44, 325–340.
Kim, K.S., et al., 2012. Hippocalcin and KCNQ channels contribute to the kinetics of the slow afterhyperpolarization. Biophys. J. 103, 2446–2454.
Kim, H.J., et al., 2016a. Protein arginine methylation facilitates KCNQ channel-PIP2 interaction leading to seizure suppression. elife 5.
Kim, K.S., et al., 2016b. The voltage activation of cortical KCNQ channels depends on global PIP2 levels. Biophys. J. 110, 1089–1098.
Kitada, T., et al., 2007. Impaired dopamine release and synaptic plasticity in the striatum of PINK1-deficient mice. Proc. Natl. Acad. Sci. U. S. A. 104, 11441–11446.
Kobayashi, M., et al., 2005. Hippocalcin-deficient mice display a defect in cAMP response element-binding protein activation associated with impaired spatial and associative memory. Neuroscience 133, 471–484.
Kobayashi, M., et al., 2012. Hippocalcin mediates calcium-dependent translocation of brain-type creatine kinase (BB-CK) in hippocampal neurons. Biochem. Biophys. Res. Commun. 429, 142–147.
Kofoed, E.M., Vance, R.E., 2011. Innate immune recognition of bacterial ligands by NAIPs determines inflammasome specificity. Nature 477, 592–595.
Krause, M., et al., 2002. Functional specificity of G alpha q and G alpha 11 in the cholinergic and glutamatergic modulation of potassium currents and excitability in hippocampal neurons. J. Neurosci. 22, 666–673.
Krishnan, A., et al., 2009. Hippocalcin, new Ca(2+) sensor of a ROS-GC subfamily member, ONE-GC, membrane guanylate cyclase transduction system. Mol. Cell. Biochem. 325, 1–14.
Lafreniere, R.G., Rouleau, G.A., 2011. Migraine: Role of the TRESK two-pore potassium channel. Int. J. Biochem. Cell Biol. 43, 1533–1536.
Lai, Y.C., et al., 2015. Phosphoproteomic screening identifies Rab GTPases as novel downstream targets of PINK1. EMBO J. 34, 2840–2861.
Larsson, H.P., 2013. What determines the kinetics of the slow afterhyperpolarization (sAHP) in neurons? Biophys. J. 104, 281–283.
Lastres-Becker, I., et al., 2016. Mammalian ataxin-2 modulates translation control at the pre-initiation complex via PI3K/mTOR and is induced by starvation. Biochim. Biophys. Acta 1862, 1558–1569.
Leroy, E., et al., 1998. The ubiquitin pathway in Parkinson's disease. Nature 395, 451–452.
Li, S., et al., 2018. Regulation of smoothened ubiquitination and cell surface expression by a Cul4-DDB1-Gbeta E3 ubiquitin ligase complex. J. Cell Sci. 131 (pii: jcs218016).
Lin, M.T., Beal, M.F., 2006. Mitochondrial dysfunction and oxidative stress in neurodegenerative diseases. Nature 443, 787–795.
Liss, B., et al., 2005. K-ATP channels promote the differential degeneration of dopaminergic midbrain neurons. Nat. Neurosci. 8, 1742–1751.
Liu, Y., et al., 2007. Calcium influx through L-type channels generates protein kinase M to induce burst firing of dopamine cells in the rat ventral tegmental area. J. Biol. Chem. 282, 8594–8603.
Liu, L., et al., 2012. Sirtuin 2 (SIRT2) enhances 1-methyl-4-phenyl-1,2,3,6-tetrahydropyridine (MPTP)-induced nigrostriatal damage via deacetylating forkhead box O3a (Foxo3a) and activating Bim protein. J. Biol. Chem. 287, 32307–32311.
Livak, K.J., Schmittgen, T.D., 2001. Analysis of relative gene expression data using real-time quantitative PCR and the 2(−Delta Delta C(T)) method. Methods 25, 402–408.
Lui, T.T., et al., 2011. The ubiquitin-specific protease USP34 regulates axin stability and Wnt/beta-catenin signaling. Mol. Cell. Biol. 31, 2053–2065.
Luthi-Carter, R., et al., 2000. Decreased expression of striatal signaling genes in a mouse model of Huntington's disease. Hum. Mol. Genet. 9, 1259–1271.
Luthi-Carter, R., et al., 2002. Dysregulation of gene expression in the R6/2 model of polyglutamine disease: parallel changes in muscle and brain. Hum. Mol. Genet. 11, 1911–1926.
Macrez-Lepretre, N., et al., 1997. Distinct functions of Gq and G11 proteins in coupling alpha1-adrenoreceptors to Ca2+ release and Ca2+ entry in rat portal vein myocytes. J. Biol. Chem. 272, 5261–5268.
Madison, D.V., Nicoll, R.A., 1984. Control of the repetitive discharge of rat CA 1 pyramidal neurones in vitro. J. Physiol. 354, 319–331.
Mammen, A., et al., 2004. Hippocalcin in the olfactory epithelium: a mediator of second messenger signaling. Biochem. Biophys. Res. Commun. 322, 1131–1139.
Manzanillo, P.S., et al., 2013. The ubiquitin ligase parkin mediates resistance to intracellular pathogens. Nature 501, 512–516.
Martella, G., et al., 2009. Enhanced sensitivity to group II mGlu receptor activation at corticostriatal synapses in mice lacking the familial parkinsonism-linked genes PINK1

or Parkin. Exp. Neurol. 215, 388–396.
Martinez, A., et al., 2017. Quantitative proteomic analysis of parkin substrates in Drosophila neurons. Mol. Neurodegener. 12, 29.
Martinez, A., et al., 2018. Neuronal proteomic analysis of the Ubiquitinated substrates of the disease-linked E3 ligases parkin and Ube3a. Biomed. Res. Int. 2018, 3180413.
Matschke, L.A., et al., 2015. A concerted action of L- and T-type Ca(2+) channels regulates locus coeruleus pacemaking. Mol. Cell. Neurosci. 68, 293–302.
Matschke, L.A., et al., 2018. Calcium-activated SK potassium channels are key modulators of the pacemaker frequency in locus coeruleus neurons. Mol. Cell. Neurosci., vol. 88, 330–341.
Mercer, E.A., et al., 2000. NAIP interacts with hippocalcin and protects neurons against calcium-induced cell death through caspase-3-dependent and -independent pathways. EMBO J. 19, 3597–3607.
Minowa-Nozawa, A., et al., 2017. Rab35 GTPase recruits NDP52 to autophagy targets. EMBO J. 36, 2790–2807.
Miura, M., et al., 2002. Group I metabotropic glutamate receptor signaling via Galpha q/Galpha 11 secures the induction of long-term potentiation in the hippocampal area CA1. J. Neurosci. 22, 8379–8390.
Moseley, A.E., et al., 2003. The Na,K-ATPase alpha 2 isoform is expressed in neurons, and its absence disrupts neuronal activity in newborn mice. J. Biol. Chem. 278, 5317–5324.
Mouton-Liger, F., et al., 2018. Parkin deficiency modulates NLRP3 inflammasome activation by attenuating an A20-dependent negative feedback loop. Glia. https://doi.org/10.1002/glia.23337. [Epub ahead of print].
Myllykoski, M., et al., 2012. The N-terminal domain of the myelin enzyme 2′,3′-cyclic nucleotide 3′-phosphodiesterase: direct molecular interaction with the calcium sensor calmodulin. J. Neurochem. 123, 515–524.
Nesbit, M.A., et al., 2013. Mutations affecting G-protein subunit alpha11 in hypercalcemia and hypocalcemia. N. Engl. J. Med. 368, 2476–2486.
Okatsu, K., et al., 2012. Mitochondrial hexokinase HKI is a novel substrate of the Parkin ubiquitin ligase. Biochem. Biophys. Res. Commun. 428, 197–202.
Ordureau, A., et al., 2015a. Defining roles of PARKIN and ubiquitin phosphorylation by PINK1 in mitochondrial quality control using a ubiquitin replacement strategy. Proc. Natl. Acad. Sci. U. S. A. 112, 6637–6642.
Ordureau, A., et al., 2015b. Quantifying ubiquitin signaling. Mol. Cell 58, 660–676.
Ordureau, A., et al., 2018. Dynamics of PARKIN-dependent mitochondrial ubiquitylation in induced neurons and model systems revealed by digital snapshot proteomics. Mol. Cell 70, 211–227 e8.
Outeiro, T.F., et al., 2007. Sirtuin 2 inhibitors rescue alpha-synuclein-mediated toxicity in models of Parkinson's disease. Science 317, 516–519.
Pahlavan, S., et al., 2012. Galphaq and Galpha11 contribute to the maintenance of cellular electrophysiology and Ca2+ handling in ventricular cardiomyocytes. Cardiovasc. Res. 95, 48–58.
Palacino, J.J., et al., 2004. Mitochondrial dysfunction and oxidative damage in parkin-deficient mice. J. Biol. Chem. 279, 18614–18622.
Palmer, C.L., et al., 2005. Hippocalcin functions as a calcium sensor in hippocampal LTD. Neuron 47, 487–494.
Pareja, F., et al., 2012. Deubiquitination of EGFR by Cezanne-1 contributes to cancer progression. Oncogene 31, 4599–4608.
Pedarzani, P., Storm, J.F., 1993. PKA mediates the effects of monoamine transmitters on the K+ current underlying the slow spike frequency adaptation in hippocampal neurons. Neuron 11, 1023–1035.
Periquet, M., et al., 2005. Proteomic analysis of parkin knockout mice: alterations in energy metabolism, protein handling and synaptic function. J. Neurochem. 95, 1259–1276.
Pino, E., et al., 2014. FOXO3 determines the accumulation of alpha-synuclein and controls the fate of dopaminergic neurons in the substantia nigra. Hum. Mol. Genet. 23, 1435–1452.
Poalas, K., et al., 2013. Negative regulation of NF-kappaB signaling in T lymphocytes by the ubiquitin-specific protease USP34. Cell Commun. Signal. 11, 25.
Ramaker, J.M., et al., 2013. Amyloid precursor proteins interact with the heterotrimeric G protein go in the control of neuronal migration. J. Neurosci. 33, 10165–10181.
Reetz, K., et al., 2008. Limbic and frontal cortical degeneration is associated with psychiatric symptoms in PINK1 mutation carriers. Biol. Psychiatry 64, 241–247.
Reyes Ruiz, V.M., et al., 2017. Broad detection of bacterial type III secretion system and flagellin proteins by the human NAIP/NLRC4 inflammasome. Proc. Natl. Acad. Sci. U. S. A. 114, 13242–13247.
Rial, D., et al., 2014. Behavioral phenotyping of Parkin-deficient mice: looking for early preclinical features of Parkinson's disease. PLoS One, vol. 9, e114216.
Rojansky, R., et al., 2016. Elimination of paternal mitochondria in mouse embryos occurs through autophagic degradation dependent on PARKIN and MUL1. elife 5.
Roszko, K.L., et al., 2017. Knockin mouse with mutant Galpha11 mimics human inherited hypocalcemia and is rescued by pharmacologic inhibitors. JCI insight 2, e91079.
Rouzier, C., et al., 2017. A novel CISD2 mutation associated with a classical Wolfram syndrome phenotype alters Ca2+ homeostasis and ER-mitochondria interactions. Hum. Mol. Genet. 26, 1599–1611.
Saitoh, S., et al., 1993. Distribution of hippocalcin mRNA and immunoreactivity in rat brain. Neurosci. Lett. 157, 107–110.
Sallese, M., et al., 2000. Regulation of G protein-coupled receptor kinase subtypes by calcium sensor proteins. Biochim. Biophys. Acta 1498, 112–121.
Sarraf, S.A., et al., 2013. Landscape of the PARKIN-dependent ubiquitylome in response to mitochondrial depolarization. Nature 496, 372–376.
Savitt, J.M., et al., 2006. Diagnosis and treatment of Parkinson disease: molecules to medicine. J. Clin. Invest. 116, 1744–1754.
Schwindt, P.C., et al., 1988. Slow conductances in neurons from cat sensorimotor cortex in vitro and their role in slow excitability changes. J. Neurophysiol. 59, 450–467.
Seirafi, M., et al., 2015. Parkin structure and function. FEBS J. 282, 2076–2088.
Shen, Z.Q., et al., 2017. CISD2 Haploinsufficiency disrupts calcium homeostasis, causes nonalcoholic fatty liver disease, and promotes hepatocellular carcinoma. Cell Rep. 21, 2198–2211.
Sliter, D.A., et al., 2018. Parkin and PINK1 mitigate STING-induced inflammation. Nature 561, 258–262.
Soman, S., et al., 2017. Inhibition of the mitochondrial calcium uniporter rescues dopaminergic neurons in pink1(-/-) zebrafish. Eur. J. Neurosci. 45, 528–535.
Song, P., et al., 2016. Parkin modulates endosomal organization and function of the Endo-Lysosomal pathway. J. Neurosci. 36, 2425–2437.
Srivastava, A., et al., 2011. The relation between depression and parkin genotype: the CORE-PD study. Parkinsonism Relat. Disord. 17, 740–744.
von Stechow, L., et al., 2015. The E3 ubiquitin ligase ARIH1 protects against genotoxic stress by initiating a 4EHP-mediated mRNA translation arrest. Mol. Cell. Biol., vol. 35, 1254–1268.
Subramaniam, M., et al., 2014. Mutant alpha-synuclein enhances firing frequencies in dopamine substantia nigra neurons by oxidative impairment of A-type potassium channels. J. Neurosci. 34, 13586–13599.
Surmeier, D.J., et al., 2012. Physiological phenotype and vulnerability in Parkinson's disease. Cold Spring Harbor Perspect. Med. 2, a009290.
Sy, S.M., et al., 2013. The ubiquitin specific protease USP34 promotes ubiquitin signaling at DNA double-strand breaks. Nucleic Acids Res. 41, 8572–8580.
Szego, E.M., et al., 2017. Sirtuin 2 enhances dopaminergic differentiation via the AKT/GSK-3beta/beta-catenin pathway. Neurobiol. Aging 56, 7–16.
Tashiro, K., et al., 2006. Suppression of the ligand-mediated down-regulation of epidermal growth factor receptor by Ymer, a novel tyrosine-phosphorylated and ubiquitinated protein. J. Biol. Chem. 281, 24612–24622.
Teckchandani, A., et al., 2014. Cullin 5 destabilizes Cas to inhibit Src-dependent cell transformation. J. Cell Sci. 127, 509–520.
Tiwari, M.N., et al., 2018. Differential contributions of Ca(2+) -activated K(+) channels and Na(+) /K(+) -ATPases to the generation of the slow afterhyperpolarization in CA1 pyramidal cells. Hippocampus 28, 338–357.
Torres-Odio, S., et al., 2017. Progression of pathology in PINK1-deficient mouse brain from splicing via ubiquitination, ER stress, and mitophagy changes to neuroinflammation. J. Neuroinflammation 14, 154.
Tran, T.A., et al., 2011. Lipopolysaccharide and tumor necrosis factor regulate Parkin expression via nuclear factor-kappa B. PLoS One 6, e23660.
Tsukiyama, T., et al., 2012. Ymer acts as a multifunctional regulator in nuclear factor-kappaB and Fas signaling pathways. Mol. Med. 18, 587–597.
Tzingounis, A.V., et al., 2007. Hippocalcin gates the calcium activation of the slow after hyperpolarization in hippocampal pyramidal cells. Neuron 53, 487–493.
Udeshi, N.D., et al., 2013. Large-scale identification of ubiquitination sites by mass spectrometry. Nat. Protoc. 8, 1950–1960.
Villalobos, C., Andrade, R., 2010. Visinin-like neuronal calcium sensor proteins regulate the slow calcium-activated after hyperpolarizing current in the rat cerebral cortex. J. Neurosci. 30, 14361–14365.
Vingill, S., et al., 2016. Loss of FBXO7 (PARK15) results in reduced proteasome activity and models a parkinsonism-like phenotype in mice. EMBO J. 35, 2008–2025.
Vives-Bauza, C., et al., 2010. PINK1-dependent recruitment of Parkin to mitochondria in mitophagy. In: Proceedings of the National Academy of Sciences of the United States of America. vol. 107. pp. 378–383.
Von Coelln, R., et al., 2004. Loss of locus coeruleus neurons and reduced startle in parkin null mice. Proc. Natl. Acad. Sci. U. S. A. 101, 10744–10749.
Wang, H., et al., 2011. Parkin ubiquitinates Drp1 for proteasome-dependent degradation: implication of dysregulated mitochondrial dynamics in Parkinson disease. J. Biol. Chem. 286, 11649–11658.
Wang, B., et al., 2017. TRAF2 and OTUD7B govern a ubiquitin-dependent switch that regulates mTORC2 signalling. Nature 545, 365–369.
Xin, D., et al., 2018. Parkin negatively regulates the antiviral signaling pathway by targeting TRAF3 for degradation. J. Biol. Chem. 293, 11996–12010.
Yamano, K., et al., 2018. Endosomal Rab cycles regulate Parkin-mediated mitophagy. elife 7.
Zhao, X.S., et al., 2001. Plasticity and adaptation of Ca2+ signaling and Ca2+ −dependent exocytosis in SERCA2(+/−) mice. EMBO J. 20, 2680–2689.
Zhao, Y., et al., 2011. The NLRC4 inflammasome receptors for bacterial flagellin and type III secretion apparatus. Nature 477, 596–600.
Zhong, Z., et al., 2016. NF-kappaB restricts inflammasome activation via elimination of damaged mitochondria. Cell 164, 896–910.
Zhu, Z., et al., 2016. Cutting edge: a cullin-5-TRAF6 interaction promotes TRAF6 polyubiquitination and lipopolysaccharide Signaling. J. Immunol. 197, 21–26.
Ziviani, E., et al., 2010. Drosophila parkin requires PINK1 for mitochondrial translocation and ubiquitinates mitofusin. Proc. Natl Acad. Sci. USA 107, 5018–5023.